Electronic structures of spinel nickel cobaltite from a spin-polarized quasi-particle self-consistent GW method

Doctoral Thesis

Electronic structures of spinel nickel cobaltite from a spin-polarized quasi-particle self-consistent GW method

スピン分極準粒子自己無撞着 GW 法による スピネル-ニッケル-コバルタイトの電子構造

Author:
Hasan al Rasyid
1724012006

Supervisor:
Professor Tatsuki Oda

A thesis submitted in fulfillment of the requirements for the degree of Doctor of Science

in the

Mathematical and Physical Sciences
Graduate School of Natural Science and Technology

KANAZAWA UNIVERSITY

Thursday 20th August, 2020 21:20

Declaration of Authorship

I, Hasan al Rasyid, declare that this thesis titled, “Electronic structures of spinel nickel cobaltite from a spin-polarized quasi-particle self-consistent GW method” (スピン分極準粒子自己無撞着 GW 法によるスピネル-ニッケル-コバルタイトの電子構造) and the work presented in it are my own. I confirm that:

- This work was done wholly or mainly while in candidature for a research degree at this University.
- Where any part of this thesis has previously been submitted for a degree or any other qualification at this University or any other institution, this has been clearly stated.
- Where I have consulted the published work of others, this is always clearly attributed.
- Where I have quoted from the work of others, the source is always given. With the exception of such quotations, this thesis is entirely my own work.
- I have acknowledged all main sources of help.
- Where the thesis is based on work done by myself jointly with others, I have made clear exactly what was done by others and what I have contributed myself.

Signed:

Date:

"Recite, and your Lord is the most Generous -
Who taught by the pen -
Taught man that which he knew not."

(Quran 96:3-5)

KANAZAWA UNIVERSITY

Abstract

Graduate School of Natural Science and Technology
Mathematical and Physical Sciences

Doctor of Science

Electronic structures of spinel nickel cobaltite from a spin-polarized quasi-particle self-consistent GW method

by Hasan al Rasyid

Quasi-particle Self-consistent GW (QSGW) calculation are performed on three probable spinel structure of $NiCo_2O_4$, i.e. two of inverse spinel structure and one normal spinel O_2. The calculation also compared with the result from Density Functional Theory (DFT) based on Generalized Gradient Approximation (GGA). The electronic states near the Fermi level consists mainly of the Nickel d band. Half metallicity is detected on all structure, and QSGW consistently show larger majority spin band gap on all spinel structure. Overall QSGW calculation yield more localized orbitals compared with that of DFT calculation. Based on Partial Density of States analysis, Co atoms have no contribution to the total magneticity the bulk system. The largest contribution to total magneticity is provided by Nickel atoms. There are some differences on magnetic arrangement of the three spinel. Among three models, the inverse spinel structure type B have the most energetically stable structure.

Acknowledgements

In the name of Allah, the Entirely Merciful, the Especially Merciful. All praises are due to my Nurturer, the Lord of the worlds. The ones that meet with His bounties and equal to His abundance. Those as befits the glory of His countenance and the greatness of His might. May He send to my beloved and most revered, the most perfect blessings and thorough salutation. To the one by whom problems are unraveled, anxieties are relieved, needs are fulfilled, aspirations are attained, good endings are revealed, and by his countenance rain descends. May He also bestow those blessings upon his family, companion, and his cord bearers, with every glance and every breath, by the number of everything that is known to The All-Knowing.

I humbly express my deepest gratitude and profound respect to my supervisor Prof. Tatsuki Oda for the incomparable support on my Doctorate study and research, for his unlimited patience, motivation, and knowledge. His thorough guidance helped me in each and every steps of this journey. May his knowledge, energy, and tenacity would always be ablaze, forging the future researchers of the coming generations.

I would also like to convey my greatest appreciation for the support of Prof. Mineo Saito, Prof. Hidemi Nagao, Prof. Sinichi Miura, and Prof. Fumiyuki Ishii, for their willingness to give a great consideration on each and every my steps, and for your endless effort to take a very careful thought on my well-beings.

My acknowledge should be addressed to the support of Japanese Government (MEXT), by means of the Program for the Development of Global Human Resources for Kanazawa University.

This thesis would be an absolute impossibility without the invaluable discussion with Dr. Masao Obata. His insights and attentions are very prized in each of its essences. I do realize his enormous efforts in presenting me many answers, which I actually have no entitlement to be granted upon.

I humbly offer my solemn prayers and recognitions to those who have guided me in my search to understand the worlds. Those who dedicated their whole life to enlight, my teachers and mentors, whose the list spans from the ones who already mentioned and on to Kanjeng Romo Kiyai H. Imam Asfali (ayh), Muhammad Iwan Tahyudin Taib (ayh) and Muhamad Abdulkadir Martoprawiro. May

your dedication and knowledge be your guidance and intercession for a shelter on the day when the sun converges.

I fully acknowledge the generosity of Dr. Indra Pardede and Dr. Nurul Ikhsan for his dedication and time in engaging many scientific exchange in our lab.

Kanazawa has become a haven, away from home, that I always keep as a dearest. All thanks to warm embrace of priceless, fabulous friends I always keep in my heart. Thank you to Yosuke Funato and Hiroto Nakano for their selfless feat in making my life in Kanazawa so enjoyable. There is no justice in this acknowledgement without mentioning my beloved Nahdlatul Ulama community, especially to Dr. Nur Hamid and Mr. Muhammad Imron. Together with many other members, we try to held this very cord by a tight and steadfast hold. May this cord bear witness to our longing heart. These yearnings, would never be quenched, and may become our beacon for his acknowledgment in the Final Day.

Contents

List of Figures

List of Tables

This thesis is dedicated to my zephyrs,
Azka Al-Adzkiya Hurriyaturrasyidah,
Zidnaftithara Nayyira Arrasyida,
Ars Muhammad Kholilurrahman,
and those who shall be named later, but never be excluded.
For they are the light, the cane, the water, and the song
in my darkest night, steepest hill, and in my schorching desolated deserts.

My passionate dedication will always find its home with
my Eka Puspita Arumaningtyas.
Yes, that is correct, for you are mine, and mine only.
This will be recorded in the whole history of this university,
and would bear witness for my obsession to you.
Please do not let this be a story like one of those infamous tattoos.

My greatest regards to my siblings and my thick companions,
Muhammad Zainal Abidin,
Nurutthoyyibah,
and Luthfiyah Wardah.
I would never be here without their kind effort and unyielding encouragement.
I have kept my ends here, eh?

Finally, I would like to convey my humblest dedication to my parents,
Arsyayadi Arsyad bin Abdurrahman
Badariyah binti Kasdam.
This thesis is a milestone of a journey, started by you both.
This milestone, essentially is not of my creations,
for it was have already been fixed in this road by your hands.

Chapter 1

Introduction

Research on Computational Sciences extends over at least three distinct areas, as illustrated in Figure **??**. Standing as an abstract tools to solve any problem ahead, we need a solid theoretical point of view. Heavily employs many advanced mathematical techniques, the theoretical base is very much consisted of novel concepts of Theoretical Physics, i.e. Quantum Physics. This theoretical base would be employed to analyze real life cases provided by experimental research. These experimental aspects are usually provided by a vast area of scientific experimentation, ranging from the fields of economy, chemistry or from the physical science itself. The third aspect, computation, plays as a bridge for theoretical constructs to carry out any means necessary for producing the quantities required for confirmation with experiment values. Nowadays, the computation is mainly performed by employing an electronical machine (a computer server). Though historically, before the dawn of programmable electronic computer, the computation was usually being done by hand, or by analog devices. Nonetheless, the development of computation techniques has been moved from a heavily mechanical physics concepts of analog machines into a more abstract mathematical concepts, indicated by various programming languages for electronical computer. One of the popular theme on this aspect is to develop a programming language that can be rigorously proven to be mathematically correct and at the same time, it should be concise and perform well in the manner of space/memory utilization and speed.

1.1 $NiCo_2O_4$

Oxygen reduction reaction (ORR) is one of the most basic reactions that construct many complex reactions such as energy generation (fuel cell), weathering of materials, and most of biological process [1]. One of the main interests of this reaction focused on its role in oxygen electrode used in electrical-power related systems, i.e. metal-air batteries and fuel cells. From this point of view, being

an abundantly available transitional metal oxides, Nickel cobaltite, $NiCo_2O_4$, have immediately shows many advantages, compared to already available alternatives. In catalysis, $NiCo_2O_4$ has a role as heterogenous catalyst with the reaction of ORR. However the mechanism of ORR on metal surfaces is still remains unclear. $NiCo_2O_4$ indicates a half-metallic property, according to low field magnetoresistance (LFMR) measurements [2]. Nickel cobaltite is also reported to be half metallic with -19.1% low-field magnetoresistance at 0.5 T and -50% at 9 T (both measured at 2 K) [2]. Combined with its high Curie temperature (295K [3], 350K [4]), these properties made nickel cobaltite into good candidate as spintronic materials. One can easily tune its electrical and magnetic properties by varying the crystal growth temperature and oxygen pressure [5]. The interest on $NiCo_2O_4$ mainly comes from its abundance and its potential use, as spintronics application, as well as alternative electrode used in electrical-power related system, i.e. metal-air batteries and fuel cells. $NiCo_2O_4$ is one of the promising materials to be used in applications of catalysis and spintronics.

$NiCo_2O_4$ is a ferrimagnet [4, 6] and one candidate of novel materials that could be engineered in many ways to exhibit different properties. By utilizing temperature growth of less than 450°C, one can acuire metallic-ferrimagnetic $NiCo_2O_4$ thin film. On the contrary, with more than 450°C, we would acquire thin film as non-magnetic insulator [7]. This uniqueness is believed to come from the competition between double exchange interaction among cations with different charges and superexchange interaction among those with same charges [3].

Electronic structure investigation from theoretical approach was reported in the work combined with the experimental measurement [8]. The authors have used a modified Becke-Jonson formula in the exchange-correlation founction based on local spin density approximation (mBJ-LDA). It reported large energy gaps of around 3−4 eV in majority spin states between the valence and conduction bands, and the result indicated a half-metallic property. The properties of electronic structure, such as large energy gap, have not been valididated yet and the details on electronic structure are not so clear that they are self-consistently understood with the properties of catalysis. The successive theoretical approach, namely LDA+U approach, introduced an on-site Coulomb parameter of Hubbard model, U_{eff}, to the cation sites [2, 5]. The results of spin-polarized density of states indicated a half-metallic property with an energy gap in the majority-spin state of about 1.3 eV. The analysis of atomic and orbital projections revealed electrons of the Ni(Oct) and Co(Tet) orbitals hybridized

with O at the Fermi level. The obtained pictures on electronic and magetic structures at the Fermi level may be based on the understanding or interpretation of many complicated experimental observations [2, 5]. This means that one can get some satisfactions from such theoretical approach on its half-metalicity. However, in those approaches, the empirical parameters were used for the U_{eff} on Ni and Co sites which were introduced as Fe spinel oxides [9]. The semiconducting/insulating property of $NiCo_2O_4$ has not been discussed from theoretical electronic structure results.

We have theoretically investigated electronic and magnetic properties of bulk $NiCo_2O_4$ to understand its basic features. In our theoretical investigation, quasi-particle self-consistent GW (QSGW) calculations [10–12] were performed in normal and inverse spinels of $NiCo_2O_4$. This method does not employ any empirical parameter like U_{eff}. {This feature} indicated a lot of advancements in the electronic structure analyses of semi-conducting and insulating materials. The QSGW calculation enables to calculate metallic electronic structures. Such advantage may be useful for a wide range of materials in the advanced methods beyond the density functional theory (DFT) [13] approach. The performance of QSGW beyond DFT in improving the electronic structure of semiconductors has been well known already [11]. The recent progress has been reached to a group of materials for power electronics [14, 15] and a group of surfaces [16]. We can find more data about applicability on its performance on wider sets of materials, i.e. half-metallic, magnetic, and metallic materials.

Half-metallic property was found on all the results of $NiCo_2O_4$ and the metallicity is associated mainly with the 3d orbitals on tetrahedral Co(tet) in the minority spin state. The QSGW investigation revealed that the Ni 3d components at the octahedral site are largely supressed at the Fermi level by a mixed valence feature with the hybridization with O 2p orbital.

1.1.1 Crystal structure and computation method

Spinel materials or their family are usually presented as a chemical formula XY_2O_4, where X and Y are cationic elements. For the cationic elements, there are two distinguishable atomic sites. They have tetrahedral and octahedral symmetries, being called tetrahedral and octahedral sites, respectively. There are 2 tetrahedral sites and 4 octahedral sites in a primitive unit cell (two formula units). In the normal spinel, all of X occupies tetragonal site and all of Y at octahedral site. In inverse spinel structure, X and Y atoms are interchanged with each other between the tetrahedral and octahedral sites. As in the previous work of $NiCo_2O_4$ [7], we considered two types of inverse spinel, called

TABLE 1.1: Configurations of tetragonal and octahedral sites for X and Y elements in spinel structure XY_2O_4. The numbers in parentheses are the number of atoms per formula unit.

system	tetrahedral site (2)	octahedral site (4)
Normal	X(2)	Y(4)
Inverse type A	X(1),Y(1)	X(1), Y(3)
Inverse type B	Y(2)	X(2), Y(2)

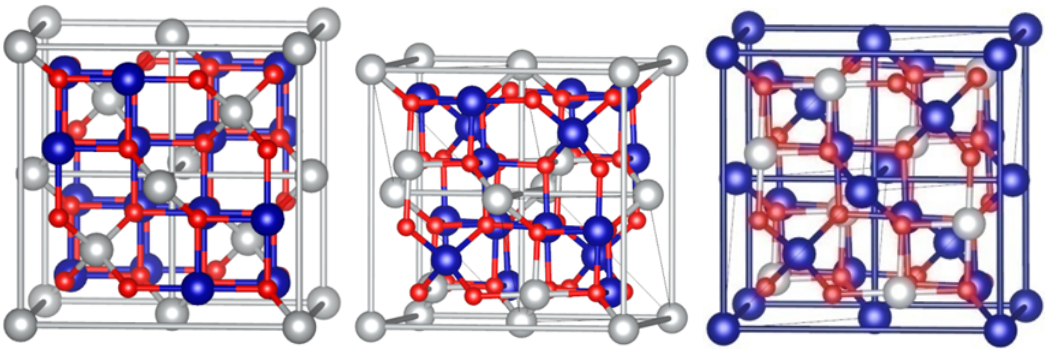

FIGURE 1.1: Three spinel structures of $NiCo_2O_4$. From left to right, they indicate spinels of normal, inverse type A, and inverse type B. Ni, Co, and O atoms are represented by silver, blue, and red color respectively.

Types A and B (inverse A and inverse B). The configurations of tetrahedral and octahedral sites for X and Y elements are presented in Table 1.1.

The crystal structure of normal spinel belongs to a faced-centered cubic structure with the space group of No. 227. In case of $NiCo_2O_4$, its structure was reported to have an inverse spinel structure [6]. We calculated normal and two inverse spinel structures of $NiCo_2O_4$. The normal and inverse spinel structures (inverse A and inverse B) are presented in Figure 1.1. Silwal *et.al.* [7] suggested that the inverse B configuration has a higher tendency to happen rather than inverse A configuration. Our discussion in this paper, particularly focused on the inverse type B.

Figure 1.2 picks up atomic configurations at the tetrahedral and octaheral sites in spinel structure. Each cation atom is surrounded by four or eight oxygen atoms depending on these site. Oxygen imposes a strong crystal field at the cation site. As a consequence of such crystal field, the five energy levels of 3d orbital will split into two kinds of levels denoted as t_{2g}(3 levels) and e_g(two levels). For the tetrahedral site surrounded by negatively charged oxygen, the

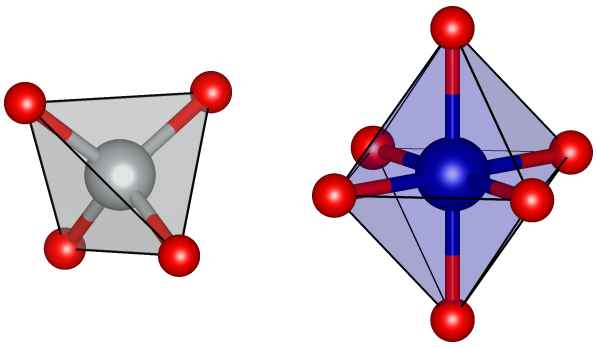

FIGURE 1.2: Atomic configurations of tetrahedral (left) and octahedral (right) sites, respectively. Silver or blue ball denotes a cation atom and red balls denote oxygen atom.

t_{2g} levels are lowered and the e_g are raised. In octahedral site, this level arrangement is reversed. The energy width of this splitting may indicate degree of the crystal field.

We investigated optimized structure of lattice parameter a and internal parameter u using the house-package of DFT(GGA) code [17] for the normal spinel structure of $NiCo_2O_4$. As u increases, the oxygen tetrahedron around the cation of tetrahedral site expands, resulting in an elongation of cation-oxygen bond. They were determined to be $a = 8.115$ Å and $u = 0.3881$. The former was in agreement with the experimental values. Thus, we decided to use the set of experimental values in our further research. Indeed, we took the experimental values of $a = 8.114$ Å and $u = 0.3833$ [6, 18]. The difference (δu) between two internal parameters presented above corresponds to an oxygen atomic distortion of 0.07 Å ($= \sqrt{3}a\ \delta u$). This is much smaller than a standard bond length of Ni-oxide (0.4%) [6].

Chapter 2

Theoretical Background

2.1 Density Functional Theory

2.1.1 Many-body system

For every system of N nuclei which each one of them positioned at R_k, we can describe a Hamiltonian of that system as:

$$\hat{\mathcal{H}} = -\sum_{i}^{N} \frac{\hbar^2}{2m_e}\nabla_i^2 + \sum_{i<j}^{N} \frac{e^2}{r_i - r_j} - \sum_{i}^{N_n} \frac{\hbar^2}{2M_i}\nabla_i^2 + \sum_{i<j}^{N_n} \frac{Z_i Z_j e^2}{R_i - R_j} + \sum_{i}^{N}\sum_{j}^{N_n} \frac{Z_j e^2}{r_i - R_j} \tag{2.1}$$

In this system, we assume that Z is electronic charge of the nuclei having a mass of M and surrounded by N electrons at position r_l with mass of me and electronic charge of e. To describe many properties of this system, we need to solve Schrodinger equation:

$$\hat{\mathcal{H}}\Psi_n(R_j, r_i) = E_n\Psi_n(R_j, r_i)$$

where Ψ is a wave function of the system state related with energy E_n.

We need to make several consideration to make a numerically simpler approach for this equation. First simplification would be based on the fact that nuclei usually much heavier than electrons in such a way that they move very slowly compared to electrons movement. This allows us to separate the movement of nuclear and electrons and then first assume that nuclei are stationary, solve the system energy and then finally reinclude the problem of nuclear motion. This assumption is the basis of Born-Oppenheimer approximation. In light of this assumption, we can rewrite the Hamiltonian as :

$$\hat{\mathcal{H}} = -\sum_{i}^{N} \frac{\hbar^2}{2m_e}\nabla_i^2 + \sum_{i<j}^{N} \frac{e^2}{r_i - r_j} + \sum_{i}^{N}\sum_{j}^{N_n} \frac{Z_j e^2}{r_i - R_j} \tag{2.2}$$

This is much more simple representation of Hamiltonian at 2.1. However, we still have many body electron-electron interaction that still contribute on huge complexity of the equation of the system with more than 3 electrons.

2.1.2 Free electron

For the next approach, we need to change our perspective on the system. Previously, we tend to see the system as a problem of the motion of N electrons in ionic potential of N_n nuclei. This perspective made us construct a huge network of equation involving sum of N x n electron coordinates. Hartree proposed different approach. We can consider that system as interaction between a given electron with all electrons remained expressed as effective potential Veff. This approach brought about an impression that each one electron have no explicit electron-electron interaction, thus leads to term of "non-interacting". We can express the effective potential as:

$$\rho(r) = \sum_{\sigma}\sum_{i} f_i^{\sigma} |\Psi_i^{\sigma}(r)|^2$$

with f_i is Fermi-Dirac distribution $\frac{1}{e^{(\varepsilon_i - \mu)/k_B T}+1}$ and σ denotes $\uparrow, \downarrow$ spin states. If we take V_{eff} as an averaged Coulomb interaction, then we can rewrite the Hamiltonian of the system at equation 2.2 as:

$$\hat{\mathcal{H}} = -\sum_{i}^{N} \frac{\hbar^2}{2m_e}\nabla_i^2 + \overbrace{e^2 \int dr' \frac{\rho(r')}{|r - r'|}}^{V_{eff}} + \sum_{i}^{N}\sum_{j}^{N_n} \frac{Z_j e^2}{r_i - R_j} \tag{2.3}$$

along with this approximation, Hartree also replaced the true N-electron wave function Ψ with a product of single-electron wavefunctions ψ.

$$\Psi(r_i, \sigma_i) = \frac{1}{\sqrt{N}} \prod_{i}^{N} \psi_i(r_i, \sigma_i)$$

with σ_i denotes spin of the electron. In this approach, the knowledge of $\rho(r)$ is essentially required. But on the other hand, to generate $\rho(r)$, we need information on the wavefunction. We can break this chicken and egg problem

by first introduce some initial guessed wavefunction (usually derived from solution of hydrogen atom). We can then use that wavefunction to construct initial density rho as a starting point to iteratively generating new effective potential and eventually new wavefunction. Ideally, this iteration can be repeated indefinitely until we procured a self-consistent wavefunction that remains unchanged in each iteration.

It is very obvious that this Hartree treatment does not consider any antisymmetry properties of fermionic particle, thus it neglects exchange interaction that required by exclusion principle. One approach to assess this problem is by introducing Slater determinant:

$$\Psi(r_i, \sigma_i) = \frac{1}{\sqrt{N!}} \begin{vmatrix} \psi_1(r_1, \sigma_1) & \cdots & \psi_1(r_N, \sigma_N) \\ \vdots & \ddots & \vdots \\ \psi_N(r_1, \sigma_1) & \cdots & \psi_N(r_N, \sigma_N) \end{vmatrix} \tag{2.4}$$

This approach is considered as Hartree-Fock approximation that would further introduced additional exchange term $V_{ex}^{i,\sigma}$ that reduce potential V_{eff} denoted as:

$$V_{ex}^{i,\sigma} = -[\sum_j \int dr' \frac{\psi_j^*(r', \sigma)\psi_j(r', \sigma)}{|r - r'|}] \frac{\psi_j(r, \sigma)}{\psi_i(r, \sigma)} \tag{2.5}$$

This approach have good performance in explaining several simple cases such as homogenous electron gas and small atoms. However, due to its inadequity to properly account correlated motion of electrons, we still need more advanced method or approximations, i.e. Density Functional Theory (DFT). Several main concepts that introduced until Hartree-Fock approximation will also be used in Density Functional Theory approach, i.e. Self-consistency, Schrodinger equation, etc.

2.1.3 Hohenberg-Kohn Theorem

In general terms, DFT stated that any property of a system of interacting particles in external potential can be explained by a functional of ground state electronic density. In more detailed manner, this theory is formulated by Hohenberg and Kohn in 1964 and they establish two basic theorems for DFT, widely known as Hohenberg-Kohn theorems [19]. The first theory stated that for any N-electron system, there is a ground-state electronic density $n(\mathbf{r})$ that is a functional of external potential $v(\mathbf{r})$. It has been proved that apart from a trivial additive constant, $v(\mathbf{r})$ is conversely a unique functional of $n(\mathbf{r})$. As an implication, $n(\mathbf{r})$ determines the obvious electron number $N = \int d^3\mathbf{r} n(\mathbf{r})$, and also external potential $v(\mathbf{r})$ and the Hamiltonian $\hat{H}$, thus everything else about

that system. The second theory stated the existence a universal functional of the density $F[n]$, which for any wavefunction generated density $n(\mathbf{r})$, we have energy functional of $E_v[n] = F[n] + \int d^3\mathbf{r} n(\mathbf{r}) v(\mathbf{r}) \geq E_g$. Using these two theorems, we can design an iterative scheme that tries to get a lower $E_v[n]$ at each of its step until it converges into some E_c. This E_c, including its related density and wavefunction, should be the ground state of the system.

2.1.4 CPVO

Car-Parrinello Method

Car-Parrinello (CP) method was proposed by Michele Parrinello and Roberto Car in 1985 as a novel method on first-principle Molecular Dynamics in a real system. This method has been successfully applied to various systems such as insulators and semiconductors. It can also applied on clusters, chemical molecules, and many relatively large system due to the simplicity of the calculation framework.

In the construction of Car-Parrinello method, we adopt Lagrangian of the system as:

$$L = \sum_{i}^{occ} m_\Phi \langle \Psi_i | \Psi_i \rangle + \frac{1}{2} \sum_I M_I R_I^2 - E_{tot}[\Psi_i, \mathbf{R}_I] + \sum_{ij}^{occ} \Lambda_{ij} (\langle \Psi_i | \Psi_j \rangle - \delta_{ij}) \tag{2.6}$$

In this Lagrangian, we assume unrestricted movement on $\mathbf{R}_I$ and virtual movement of Ψ_i. The kinetic energy of those two movements are represented in first and second term of equation 2.6. M_I and m_Φ are atomic mass and fictious mass of wavefunction. The third term of this Lagrangian is the external potential energy (from the point of view of electron), that in ground state of related electronic system, would be very much equal with the potential of the atoms. The last term imposes normalization constraint on the wavefunction with Λ is a Lagrange multiplier. Here, Λ is a Hermitian matrix.

Furthermore, we have total energy of the system E_{tot}, reported in `vofrho.f`, deduced from Density Functional Theory as:

$$Etot[\Psi_i, R_I] = \sum_i^{occ} \langle \Psi_i | -\frac{1}{2}\nabla^2 + V_{NL} | \Psi_i \rangle + \frac{1}{2} \int\int \frac{n(r)n(r')}{|r-r'|} dr dr' + \int V_{loc}(r) n(r) dr + E_{xc} + \frac{1}{2} \sum_{I,I'}^{I \neq I'} \frac{Z_I Z_{I'}}{R_I - R_{I'}}$$

with electron density as:

$$n(r) = \sum_i^{occ.} |\Psi_i(r)|^2$$

In this total energy formula, we separate potential of nuclei as the non-local part and local part (V_{NL} and V_{loc}) due to our decision to employ pseudopotential in our construction.

The Euler-Lagrange equation derived from above Lagrangian would be

$$m_\Psi \ddot{\Psi}_i(r) = -(\mathcal{H}\Psi_i)(r) + \sum_j^{occ.} \Lambda_{ij} \Psi_j(r) \tag{2.7}$$

$$M_I \ddot{R}_I = -\frac{dE_{tot}}{dR_I} = F_I \tag{2.8}$$

Both equation denoting Force that imposed on all electrons and that of fictious force on wavefunction. The Kohn-Sham Hamiltonian $\mathcal{H}$ is defined by

$$\mathcal{H} = -\frac{1}{2}\nabla^2 + V_{NL} + \overbrace{V_{loc} + V_H + V_{xc}}^{V_{eff}}$$

with

$$V_H(r) = \int \frac{n(r')}{|r-r'|} dr'$$

$$V_{xc} = \frac{\delta E_{xc}}{\delta n(r)}$$

Here, we assume that Λ is already diagonalized and thus we have construction for Φ as

$$\mathcal{H} |\Phi_i\rangle = \varepsilon_i |\Phi_i\rangle$$

Φ and Ψ is conneceted by a unitary transformation utilizing a unitary matrix T following:

$$\Phi_l = \sum_i (T^\dagger)_{li} \Psi_i$$

To solve the equation of motion in 2.8, we need the normalized orthogonal condition of $\langle \Psi_i | \Psi_j \rangle = \delta_{ij}$. When Ψ is in ground state, the force on atom at position R_I is accurately follows Hellmann-Feynman theorem. If we use ultra-soft pseudopotential, we need additional term in atomic force formulation at equation 2.8.

Practically, in Car-Parrinello method, the equation of motion in 2.8 is differentiated and solved numerically. One of popular technique is by employing Verletśmethod following:

$$\Psi_i(t + \Delta t) = 2\Psi_i(t) - \Psi_i(t - \Delta t) + \frac{(\Delta t)^2}{m_\Psi}(-\mathcal{H}\Psi_i(t) + \sum_j^{occ.} \Lambda_{ij}\Psi_j(t)) \quad (2.9)$$

$$R_i(t + \Delta t) = 2R_I(t) - R_I(t - \Delta t) + \frac{(\Delta t)^2}{M_I} F_I \quad (2.10)$$

At each iteration of t, we can immediately calculate all terms for the wave-function and force, excluding Λ_{ij} term. We then assume that Λ_{ij} follows standard orthogonalization condition at time $t + \Delta t$, stated as:

$$\langle \Psi_i(t + \Delta t) | \Psi_j(t + \Delta t) \rangle = \delta_{ij} \quad (2.11)$$

Following the definition of Ψ_i in Verlet as:

$$\bar{\Psi}_i(t) = 2\Psi_i(t) - \Psi_i(t - \Delta t) - \frac{(\Delta t)^2}{m_\Psi}\mathcal{H}\Psi_i(t)$$
$$\Psi_i(t + \Delta t) = \bar{\Psi}_i(t) + \sum_j^{occ.} \frac{(\Delta t)^2}{m_\Psi}\Lambda_{ij}\Psi_i(t)$$

and combine them with orthogonalization condition at 2.11 into identity

$$A + X * B + (X * B)^\dagger + X * X^t = 1$$

we would have these agreement on

$$A_{ij} = \langle \bar{\Psi}_i | \bar{\Psi}_j \rangle$$
$$B_{ij} = \langle \Psi_i | \bar{\Psi}_j \rangle$$
$$X_{ij} = \frac{(\Delta t)^2}{m_\Psi} \Lambda_{ij}$$

By then, the Lagrange multiplier Λ_{ij} can be calculated.

The flow of Car-Parrinello technique then can be described as follows. Initially, we define arbitrary wave function from which we calculate initial electron density. Then we acquire potential of electrons and evaluates the equation of motion in 2.8. Using these forces (fictious for wavefunction), we generate new set of wavefunction and atomic coordinates. At ground state, we should expect R_I to move following lowest energy mode of vibration. In this case, we would have wavefunction to be converged into ground-state.

The Lagrangian of this scheme would follows an energy conservation requirements

$$E_{const.} = \sum_i^{occ.} m_\Phi \langle \dot{\Psi}_i | \dot{\Psi}_i \rangle + \frac{1}{2} \sum_i M_I \dot{R}_I^2 + E_{tot}[\Psi_i, R_I]$$

On the other hand, we may fix the position of atoms, and the equation of fictious motion of the wavefunctions can be performed. We should consider the fictious friction term that is proportional to the velocity of the wave function. By reducing the kinetic energy of the wave function, the system can smoothly converges to the ground state. Considering this fictious friction, we may update the equation 2.10 into

$$\Psi_i(t + \Delta t) = \frac{2}{1+\tau} \Psi_i(t) - \frac{1-\tau}{1+\tau} \Psi_i(t - \Delta t) + \frac{1}{1+\tau} \frac{(\Delta t)^2}{m_\Psi} (-\mathcal{H} \Psi_i(t) + \sum_j^{occ.} \Lambda_{ij} \Psi_j(t))$$

Practically, we may define τ between 0.15 to 0.005, or smaller value when we near convergence.

long story short, we would have:

(2.12)

(2.13)

2.1.5 Ultrasoft Pseudopotential

$$n(r) = \sum_{i}^{occ.} |\Psi_i(r)|^2 + \sum_{nmI} Q^I_{nm}(r) \langle \beta^I_n | \Psi_i \rangle \langle \Psi_i | \beta^I_m \rangle \tag{2.14}$$

$$\mathcal{H} = -\frac{1}{2}\nabla^2 + VNL + V_{eff} + \sum_{nmI} |\beta^I_m\rangle D^I_{nm} \langle \beta^I_m| \tag{2.15}$$

$$V_{eff}(r) = V_{loc}(r) + \int \frac{n(r')}{|r - r'|} dr' + V^N_{xc}(r) \tag{2.16}$$

$$D^I_{nm} = D^{(0)I}_{nm} + \int Q^I_{nm}(r) V_{eff}(r) dr \tag{2.17}$$

$$V_{NL} = \sum_{nmI} |\beta^I_m\rangle D^{(0)I}_{nm} \langle \beta^I_m| \tag{2.18}$$

$$\langle \Psi_i | S | \Psi_j \rangle = \delta_{ij} \tag{2.19}$$

$$S = 1 + \sum_{nmI} q^I_{nm} |\beta^I_m\rangle \langle \beta^I_n| \tag{2.20}$$

$$q^I_{nm} = \int Q^I_{nm}(r) dr \tag{2.21}$$

$$\sum_{ij}^{occ.} \Lambda_{ij} (\langle \Psi_i | S | \Psi_j \rangle - \delta_{ij}) \tag{2.22}$$

$$F_I = -\frac{\partial E_{tot}}{\partial R_I} + \sum_{ij}^{occ.} \Lambda_{ij} \langle \Psi_i | \frac{\partial S}{\partial R_I} | \Psi_j \rangle \tag{2.23}$$

$$F_I = -\sum_{nm} (D^I_{nm} \frac{\partial \rho^I_{nm}}{\partial R_I}) \tag{2.24}$$

$$- \int dr (Veff(r)) \sum_{nm} \frac{dQ^I_{nm}(r)}{dR_I} \rho^I_{nm} \tag{2.25}$$

$$- \int drn(r) \frac{dV^{ion}_{loc}(r)}{dR_I} - \frac{dU_{ion}}{dR_I} \tag{2.26}$$

$$+ \sum_{nm} q^I_{nm} \frac{\partial \omega^I_{nm}}{\partial R_I} \tag{2.27}$$

$$\rho^I_{nm} \equiv \sum_i^{occ.} \langle \beta^I_n | \psi_i \rangle \langle \psi_i | \beta^I_m \rangle \tag{2.28}$$

$$\omega^I_{nm} \equiv \sum_{ij}^{occ.} \Lambda_{ij} \langle \psi_i | \beta^I_m \rangle \langle \beta^I_n | \psi_j \rangle \tag{2.29}$$

$$\frac{\partial \rho^I_{nm}}{\partial R_I} \equiv \sum_i^{occ.} \langle \frac{\partial \beta^I_n}{\partial R_I} | \psi_i \rangle \langle \psi_i | \beta^I_m \rangle + \langle \beta^I_n | \psi_i \rangle \langle \psi_i | \frac{\partial \beta^I_m}{\partial R_I} \rangle \tag{2.30}$$

$$\frac{\partial \omega^I_{nm}}{\partial R_I} \equiv \sum_{ij}^{occ.} \Lambda_{ij} \langle \psi_i | \frac{\partial \beta^I_m}{\partial R_I} \rangle \langle \beta^I_n | \psi_j \rangle + \langle \psi_i | \beta^I_m \rangle \langle \frac{\partial \beta^I_n}{\partial R_I} | \psi_j \rangle \tag{2.31}$$

Force calculation

$$n(r) = \sum_k f_k |\Phi_k(r)|^2 \tag{2.32}$$

$$f_k = w_k q_k \tag{2.33}$$

$$q_k = \frac{1}{e^{\beta(\varepsilon_k - \mu)+1}} \tag{2.34}$$

$$F_{tot} = E_{tot}[\Phi_k, \varepsilon_k . R_I] - \frac{1}{\beta} S_{el} \tag{2.35}$$

$$S_{el} = -\sum_k w_k q_k ln q_k + (1^q_k) ln(1 - q_k) \tag{2.36}$$

xxxx

$$\frac{\delta}{\delta f_k} F_{tot} - \mu(\sum_l f_l - N_e) = -(\varepsilon_k - \langle \Phi_k | \mathcal{H} | \Phi_k \rangle) = 0 \tag{2.37}$$

$$\frac{\delta E_{tot}}{\delta f_k} = \langle \Phi_k | \mathcal{H} | \Phi_k \rangle \tag{2.38}$$

$$\frac{\delta E_{tot}}{\delta f_k} = -(\varepsilon_k - \mu) \tag{2.39}$$

$$f_k = w_k \bar{\theta}(x_k), x_k = (\mu - \varepsilon_k)/\sigma \tag{2.40}$$

$$E_{en} = \sigma \sum_k w_k \bar{\theta}_1(x_k) \tag{2.41}$$

$$\bar{\theta}_1(x) = \int_{-inf}^{x} y \bar{\delta}(y) dy \tag{2.42}$$

$$\bar{\delta}(x) = \frac{d\bar{\theta}(x)}{dx} \tag{2.43}$$

$$MP\bar{\theta}(x) = \frac{1}{2}1 + sgn(x)erf(|x|) + \frac{1}{2\sqrt{\pi}}xe^{-x^2} \tag{2.44}$$

$$GA\bar{\theta}(x) = \frac{1}{2}1 + sgn(x)erf(|x|) \tag{2.45}$$

$$erf(x) = \frac{2}{\sqrt{\phi}}\int_0^x e^{-y^2}dy \tag{2.46}$$

$$m_\Phi \ddot{\Phi}_k(r) = -(\mathcal{H}\Phi_k)(r) + \sum_l \frac{1}{f_k}\Lambda_{kl}\Phi_l(r) \tag{2.47}$$

$$\mathcal{L}_\Phi = \sum_k m_\Phi f_k \langle\bar{\Phi}_k|\bar{\Phi}_k\rangle - F_{tot}[\Phi_k, \varepsilon_k, R_I] + \sum_{kl}\Lambda_{kl}(\langle\Phi_k|\Phi_l\rangle - \delta_{kl}) \tag{2.48}$$

$$f_k(\mathcal{H}\Phi_k)(r) = \sum_l \Lambda_{kl}\Phi_l(r) \tag{2.49}$$

$$f_k \langle\Phi_l|\mathcal{H}|\Phi_k\rangle = \Lambda_{kl} \tag{2.50}$$

$$(f_k - f_l)\langle\Phi_l|\mathcal{H}|\Phi_k\rangle = 0 \tag{2.51}$$

$$\sum_j f_{ij}\langle\Psi_j|\mathcal{H}|\Psi_{i'}\rangle - \langle\Psi_i|\mathcal{H}|\Psi_j\rangle f_{ji'} = 0 \tag{2.52}$$

$$f^*_{ij} = \sum_k (U)_{ik} f_k (U^\dagger)_{kj} \tag{2.53}$$

$$n(r) = \sum_{ij} f_{ij}\Psi^*_i(r)\Psi_j(r) \tag{2.54}$$

$$F_I = -\frac{d}{dR_I}F_{tot} - \mu(\sum_l f_l - N_e) \tag{2.55}$$

$$= -\frac{\partial F_{tot}}{\partial R_I} - \sum_k \frac{\partial}{\partial f_k}F_{tot} - \mu(\sum_l f_l - N_e)\frac{df_k}{dR_I} \tag{2.56}$$

$$F_I = -\frac{\partial F_{tot}}{\partial R_I} \tag{2.57}$$

Verlet Method

$$m_\Phi \ddot{\Phi}_k = -\mathcal{H}\Phi_k + \sum_l \Lambda_{kl}\Phi_l - m_\Phi \dot{x}_e \dot{\Phi}_k \tag{2.58}$$

$$M_I \ddot{R}_I = F_I - M_I \dot{R}_I \dot{x}_R \tag{2.59}$$

$$Q_e \ddot{x}_e - 2(E_{kin} - E_{kin0}) \tag{2.60}$$

$$Q_n \ddot{x}_R = 2(K_R - \frac{1}{2} g_R k_B T_{ex}) \tag{2.61}$$

$$m_\varepsilon \ddot{\varepsilon}_{ij} = -(\varepsilon_{ij} - \langle \Psi_i | \mathcal{H} | \Psi_j \rangle) \tag{2.62}$$

$$2\pi\sqrt{m_\varepsilon} \tag{2.63}$$

$$m_\Phi \ddot{\Phi}_k = -\mathcal{H}\Phi_k + \sum_l \frac{1}{f_k}\Lambda_{kl}\Phi_l - m_\Phi \dot{x}_e \dot{\Phi}_k \tag{2.64}$$

$$M_I \ddot{R}_I = F_I - M_I \dot{R}_I \dot{x}_R \tag{2.65}$$

$$\mathcal{H}\Phi_k = \frac{1}{f_k}\frac{\delta F_{tot}}{\delta \Phi_k^*} \tag{2.66}$$

$$F_I = -\frac{\partial F_{tot}}{\partial R_I} \tag{2.67}$$

$$T^\dagger(\varepsilon^t)T = \varepsilon^d \tag{2.68}$$

$$f_l^d = w_l q_l = \frac{w_l}{e^{\beta(\varepsilon_l^d - \mu)} + 1} \tag{2.69}$$

$$f_{ij} = T(f^d)T^\dagger \tag{2.70}$$

$$\Lambda_{lk} = \frac{2f_k f_l}{f_k + f_l}\langle \Psi_k | H | \Psi_l \rangle - m_\Psi \langle \dot{\Psi}_k | \Psi_l \rangle + \frac{1}{2} m_\Psi \frac{d^2}{dt^2} \langle \Psi_k | \Psi_l \rangle \tag{2.71}$$

$$\frac{f_k + f_l}{2f_k f_l}\Lambda_{lk} - \langle \Psi_k | H | \Psi_l \rangle + m_\Psi \langle \dot{\Psi}_k | \dot{\Psi}_l \rangle = 0 \tag{2.72}$$

$$m_\Psi \frac{d^2}{dt^2} \langle \Psi_k | \Psi_l \rangle = 0 \tag{2.73}$$

$$\langle \Psi_k | \Psi_l \rangle = c_{kl} t + d_{kl} \tag{2.74}$$

$$\begin{aligned} \Psi_i(t + \Delta t) = {} & 2\Psi_i(t) - \Psi_i(t - \Delta t) \\ & - \frac{(\Delta t)^2}{m_\Psi} (H\Psi_j)(t) + \frac{(\Delta t)^2}{m_\Psi} \sum_j \frac{1}{f_i} \Lambda_{ij}(t + \Delta t)(S\Psi_j)(t) \end{aligned}$$

$$\begin{aligned} R_I(t + \Delta t) = {} & 2R_I(t) - R_I(t - \Delta t) \\ & - \frac{(\Delta t)^2}{M_I} \frac{\partial E_{tot}(t)}{\partial R_I} + \frac{(\Delta t)^2}{M_I} \sum_{ij} \Lambda_{ij}(t + \Delta t) \langle \Psi_i(t) | \frac{\partial S(t)}{\partial R_I} | \Psi_j(t) \rangle \end{aligned}$$

$$\langle \Psi_i(t + \Delta t) | S(t + \Delta t) | \Psi_j(t + \Delta t) \rangle = \delta_{ij} \tag{2.75}$$

$$A + YB + (YB)^\dagger + YCY^\dagger = 1 \tag{2.76}$$

$$Y_{ij} = \frac{(\Delta t)^2}{m_\Psi} \frac{1}{f_i} \Lambda^*_{ij}(t + \Delta t) \tag{2.77}$$

$$A_{ij} = \langle \bar{\Psi}_i | S(t + \Delta t) | \bar{\Psi}_j \rangle \tag{2.78}$$

$$B_{ij} = \langle \hat{\Psi}_i | S(t + \Delta t) | \bar{\Psi}_j \rangle \tag{2.79}$$

$$C_{ij} = \langle \hat{\Psi}_i | S(t + \Delta t) | \hat{\Psi}_j \rangle \tag{2.80}$$

$$\bar{\Psi}_i \equiv 2\Psi_i(t + \Delta t) - \Psi_i(t) - \frac{(\Delta t)^2}{m_\Psi} (H\Psi_i)(t) \tag{2.81}$$

$$\hat{\Psi}_i \equiv (S\Psi_i)(t) \tag{2.82}$$

$$\Lambda^{(0)}_{ij}(t + \Delta t) = 2\Lambda_{ij}(t) - \Lambda_{ij}(t - \Delta t) \tag{2.83}$$

$$f_i Y_{ij} = f_j Y_{ji}^* \tag{2.84}$$

$$(Y_a)_{ij} = -\frac{f_i - f_j}{f_i + f_j}(Y_h)_{ij} \tag{2.85}$$

$$Y^{(0)}B_h + (Y^{(0)}B_h)^\dagger = 1 - A \tag{2.86}$$

$$Y^{(0)}B_h + (Y^{(0)}B_h)^\dagger = 1 - A \tag{2.87}$$

$$Y_h^{(0)} = UZU^\dagger \tag{2.88}$$

$$Z_{kl} = \frac{(U^\dagger(1-A)U)_{kl}}{\lambda_k + \lambda_l} \tag{2.89}$$

$$\begin{aligned} Y_h^{(n+1)}B_h + (Y_h^{(n+1)})^\dagger = 1 - A - Y^{(n)}B_a - (Y^{(n)}B_a)^\dagger \\ - Y_a^{(n)}B_h - (Y_a^{(n)}B_h)^\dagger - Y^{(n)}C(Y^{(n)})^\dagger \end{aligned}$$

$$\Lambda_{ij}^*(t + \Delta t) = \frac{m_\Psi}{(\Delta t)^2}\frac{2f_i f_j}{f_i + f_j}(Y_h)_{ij} \tag{2.90}$$

$$\langle \Psi_i | H | \Psi_j \rangle = \frac{2}{f_i + f_j}\Lambda_{ij}^* = \frac{2}{f_i + f_j}\Lambda_{ji} = \frac{m_\Psi}{(\Delta t)^2}\frac{4f_i f_j}{(f_i + f_j)^2}(Y_h)_i j \tag{2.91}$$

Expansion at Periodic System

$$\sum_k^{occ.} \langle \dot{\Psi}_k | \dot{\Psi}_k \rangle \, m_\Psi = 2m_\Psi \frac{k_B T}{M} \sum kocc. \, \langle \Psi_k | - \frac{1}{2}\nabla^2 | \Psi_k \rangle \tag{2.92}$$

$$\Phi_k(r,t) = \frac{1}{\sqrt{\Omega}} \sum_G C_k(G) e^{iG\cdot(r - R_I)} e^{iG\cdot R_I(t)} \tag{2.93}$$

$$R_I(t + \Delta t) \approx R_I(t) + \dot{R}_I(t)\Delta t \tag{2.94}$$

$$\dot{\Phi}_k(r,t) = \frac{1}{\sqrt{\Omega}} \sum_G C_k(G) e^{iG\cdot(r - R_I)} \sum_I (iG) \cdot \dot{R}_I(t) e^{iG\cdot R_I(t)} \tag{2.95}$$

2.2 Elementary Concepts

To bring our understandings on the theoretical base of quasi-particle GW method, we should enrich our understanding in some concepts borrowed from Quantum Electrodynamics. In this frame, we may work in quantum mechanical paradigm, by :

1. calculate a wave function and then apply a quantum operators to find some expected physical quantities, or
2. directly consider amplitudes for a given process.

The first way is the usual way that we may found in DFT or HF approach. Now, we need to emphasize on the second way, to directly consider the amplitudes for a given process. To be specific, we take a consideration of "The amplitude that a particular particle starts at point y at a time t_y" and ends up at point x at time t_x ". This consideration would have a representation of $\langle x(t_x)|y(t_y)\rangle$, or in general we may say $\langle final|initial\rangle$. We call this amplitude as a *propagator*. Using this representation, we will have a propagator as an alternative for wave functions, in such a way that by having a propagator, we can extract all information that can be acquired by a wave function.

There are several important points that can be achieved using propagators. 1. wave functions are special cases of propagators and contain less information 2. Propagator represent the most economical way to calculate all of the properties of quantum fields in an interacting system of many particles 3. propagators for single particles have a neat property: its a Green's functions of the equation of motion for a particle.

2.3 Green's Function G

For a general linear differential operator $\hat{L}$: $\hat{L}x(t) = f(t)$ we will define the Green's function $G(t,u)$ of $\hat{L}$ as: $\hat{L}G(t,u) = \delta(t-u)$.

In the first grade term, we may have a linear differential equation from an oscillator with mass m and spring constant K evolving under the influence of a time-dependent force $f(t)$.

$$m\frac{d^2}{dt^2}x(t) + Kx(t) = f(t), \text{linear operator as:} \hat{L} = m\frac{d^2}{dt^2} + K \tag{2.96}$$

Our approach to solve this problem, can be as simple as summing up many small delta functions to make force function $f(t)$: $f(t) = \int_0^\infty du f(u)\delta(t-u)$

with u is a dummy to break up force into delta. This superposition is good because $\hat{L}$ is linear.

To solve this problem, we will consider only one delta function and try to solve $f(t)$ for single delta function. $\left[m\frac{d^2}{dt^2}+K\right]G(t,u)=\delta(t,u)$ with G(t,u) is our solution and called Green's function. From here on, we can consider the full solution $x(t)$ as an integral of Green's function weighted by the force function f(u). $x(t)=\int_0^\infty duG(t,u)f(u)$ By following back that :

$$\hat{L}x(t) = \int du\hat{L}G(t,u)f(u) \tag{2.97}$$

$$= \int du\delta(t-u)f(u) \tag{2.98}$$

$$= f(t) \tag{2.99}$$

We can solve an inhomogenous differential equation by finding the Green's function G(t,u) and then integrating over f(u) to get the solution x(t). Thus, G will need two arguments: our variable of interest and a dummy variable for delta function to build up inhomogenous part of the equation ($f(t)$). And our problem become finding the Green's function of our common $\hat{L}$.

Propagators

For every wave function $\phi(x,t)$, we have Schrödinger equation $\hat{H}\phi(x,t)=i\frac{\partial\phi(x,t)}{\partial t}$ with $\hat{H}$ is an operator function of x that governs the evolution/change of ϕ.

On the other hand, we have a Green's function that have a property of:

$$x(t)=\int_0^\infty du\ G(t,u)f(u)\ \phi(x,t_x)=\int dy\ G^+(x,t_x,y,t_y)\psi(y,t_y) \tag{2.100}$$

Based on this equation, we may construct several stories (with the same substance):

1. Green's function takes a wave function at y spacetime, and evolves it to t spacetime. To find out how this evolution behaves, we need to integrate over space.
2. the Green's function **propagates** the particle from spacetime (y,t_y) to (x,t_x), thus said *propagator*.
    1. We also add a constrain G to only $t_x>t_y$, and $\forall t_x<t_y, G=0$, to prevent propagation back in time.
    2. Thus we have *time-retarded* Green's function, G^+.

3. If we interpret $\psi(n, t_n)$ as the amplitude to find a particle at spacetime (n, t_n). Then, it follows that the propagator $G^+(x, t_x, y, t_y)$ is the probability amplitude that a particle in state $|y\rangle$ at time t_y ends up in a state $|x\rangle$ at time t_x. Thus the Green's function may be written as: $G^+(x, t_x, y, t_y) = \theta(t_x - t_y) \langle x(t_x)|y(t_y)\rangle$ Using this interpretation, we found that time variable already handled by Green's function, so we do not need to integrate previous ϕ over time. Under this interpretation, we also have wave function $\phi(x, t_x) = \langle x|\psi(t)\rangle$ as the amplitude that a particle is found at a particular spacetime of (x, t_x), without any info on its starting point.

We may process propagator $G^+(x, t_x, y, t_y) = \theta(t_x - t_y) \langle x(t_x)|y(t_y)\rangle$ in such a way that the time dependence is taken away from the states:

$$\begin{aligned} G^+(x, t_x, y, t_y) &= \theta(t_x - t_y) \langle x(t_x)|y(t_y)\rangle && (2.101)\\ &= \theta(t_x - t_y) \langle x|\hat{U}(t_x - t_y)|y\rangle && (2.102)\\ &= \theta(t_x - t_y) \langle x|e^{-i\hat{H}(t_x - t_y)}|y\rangle && (2.103) \end{aligned}$$

then we can continue to expand the amplitudes in terms of the eigenstates of the $\hat{H}$, which we call $|n\rangle$ having eigenvalues of E_n.

$$\begin{aligned} G^+(x, t_x, y, t_y) &= \theta(t_x - t_y) \langle x|e^{-i\hat{H}(t_x - t_y)}|y\rangle && (2.104)\\ &= \theta(t_x - t_y) \sum_n \langle x|e^{-i\hat{H}(t_x - t_y)}|n\rangle \langle n|y\rangle \text{ using } 1 = \sum_n |n\rangle \langle n| && (2.105) \end{aligned}$$

Following that $\langle x|n\rangle$ is a wave function of $\phi_n(x)$, we finally have the propagator written in terms of the eigenfunctions of $\hat{H}$:

$$G^+(x, t_x, y, t_y) = \theta(t_x - t_y) \sum_n \psi_n(x)\psi_n^*(y)e^{-iE_n(t_x - t_y)} \quad (2.106)$$

Thus we have relation of wave functions and propagators.

Next, we expand our assumption into a confirmation that the propagator $G^+(x, t_x, y, t_y)$ is indeed a Green's function of Schrödinger equation. To do that, we define for Schrödinger equation, the Green's function $G^+(x, t_x, y, t_y)$ is a function of x and t_x only, while y and t_y are dummies. In this regards, we would have $\hat{H}$ is a function of x, t_x

$$\left[\hat{H}_x - i\frac{\partial}{\partial t_x}\right] G^+(x,t_x,y,t_y) = -i\delta(x-y)\delta(t_x-t_y) = -i\delta^{(2)}(x-y) \quad (2.107)$$

then, our aim is to confirm that the amplitude $\langle x(t_x)|y(t_y)\rangle$ is truly the Green's function of the Schrödinger equation.

$$G^+(x,t_x,y,t_y) = \theta(t_x-t_y)\,\langle x(t_x)|y(t_y)\rangle = \theta(t_x-t_y)\sum_n \psi_n(x)\psi_n^*(y)e^{-iE_n(t_x-t_y)} \quad (2.108)$$

we can have:

$$\left[\hat{H}_x - i\frac{\partial}{\partial t_x}\right] G^+(x,t_x,y,t_y) = -i\delta(x-y)\delta(t_x-t_y) = -i\delta^{(2)}(x-y)$$

$$\left[\hat{H}_x - i\frac{\partial}{\partial t_x}\right] \theta(t_x-t_y)\sum_n \psi_n(x)\psi_n^*(y)e^{-iE_n(t_x-t_y)} = -i\delta(x-y)\delta(t_x-t_y) = -i\delta^{(2)}(x-y)$$

we do in two stages, first we have:

$$\text{using } \frac{\partial}{\partial t_x}\theta(t_x-t_y) = \delta(t_x-t_y) \text{ and } duv = udv + vdu \quad (2.109)$$

$$i\frac{\partial}{\partial t_x}G^+ = i\delta(t_x-t_y)\sum_n \psi_n(x)\psi_n^*(y)e^{-iE_n(t_x-t_y)} \quad (2.110)$$

$$+\,\theta(t_x-t_y)\sum_n E_n\psi_n(x)\psi_n^*(y)e^{-iE_n(t_x-t_y)} \quad (2.111)$$

second stage, we consider:

$\hat{H}_x$ only acts on the Green's function, and using $\hat{H}_x\psi_n(x) = E_n\psi(x)$

$$\begin{aligned}\hat{H}_xG^+ &= \hat{H}_x\theta(t_x-t_y)\,\langle x(t_x)|y(t_y)\rangle = \theta(t_x-t_y)\,\langle x(t_x)|y(t_y)\rangle \\ &= \theta(t_x-t_y)\sum_n E_n\psi_n(x)\psi_n^*(y)e^{-iE_n(t_x-t_y)}\end{aligned}$$

finally, we combine them into:

$$\left[\hat{H}_x - i\frac{\partial}{\partial t_x}\right] G^+(x,t_x,y,t_y) = -i\delta t_x - t_y\sum_n \psi_n(x)\psi_n^*(y)e^{-iE_n(t_x-t_y)} \quad (2.112)$$

$$= -i\delta(t_x-t_y)\delta(x-y) \quad (2.113)$$

Green's function in frequency/energy domain is noted as:

$$G^{+}(x,y,E) = \sum_{n} \frac{i\psi_n(x)\psi_n^*(y)}{E - E_n} \tag{2.114}$$

Two distinct feature of this equation is: 1. the singularities on the real axis occur when parameter E equals energies of the eigenstates $\psi_n(x)$, stated as $E = E_n$ 2. The residues as the singularities are $(i*)$ the wave functions.

To see the contribution of Green's function in perturbation problem, we will consider original Green's function equation in a symbolic and matrix-like form as (H-E)G=-1, where G is describing propagation of particle from y to x. This symbolic Green's function equation is solved by $G = \frac{1}{E-H}$ that similiar with:

$$G^{+}(x,y,E) = lim_{\varepsilon->0^{+}} \sum_{n} \frac{i\psi_n(x)\psi_n^*(y)}{E - E_n + i\varepsilon} \tag{2.115}$$

To solve perturbation problem (i.e. $H = H_0 + V$, where H_0 is solvable part and V is perturbing potential) using Green's function, we should see: 1. the solvable part of the problem as a particle propagating from point to point. 2. the perturbation V as a *scattering process* that interrupts the propagation.

We can illustrate this view as $G = \frac{1}{E-H_0-V}$ for $H = H_0 + V$.

In perturbation problems, G is *full propagator*. The solvable part of the Hamiltonian H_0 can be expressed as $G_0 = \frac{1}{E-H_0}$ (it means we can find the Green's function for H_0) Subscript of "0" means free propagating particle, with no scattering. Thus we call G_0 as *free propagator*. Then, using matrix identity of

$$\frac{1}{A+B} = \frac{1}{A} - \frac{1}{A}B\frac{1}{A} + \frac{1}{A}B\frac{1}{A}B\frac{1}{A} - ...$$

$$G = \frac{1}{E - H_0 - V} = \frac{1}{E-H_0} + \frac{1}{E-H_0}V\frac{1}{E-H_0} + \frac{1}{E-H_0}V\frac{1}{E-H_0}V\frac{1}{E-H_0} + ...$$

$$G = G_0 + G_0VG_0 + G_0VG_0VG_0 + G_0VG_0VG_0G_0VG_0 + ...$$

Even though we cannot calculate $1/(E - H_0 - V)$, we can calculate $1/(E - H_0)$ as G_0, and expect G to be approximated by few terms.

So in conclusion, we can view perturbation problems into a simple terms of G_0VG_0. Diagrammatically, this problem is shown is Figure 2.1. This diagram is a representation of mathematical formula shown in Equation 2.116.

Back to the expansion of equation 2.116, we have found that perturbation problem can be expressed as a simple picture of particle scattering. The amplitude for a particle to go from y to x is G. The same G, is a superposition of the

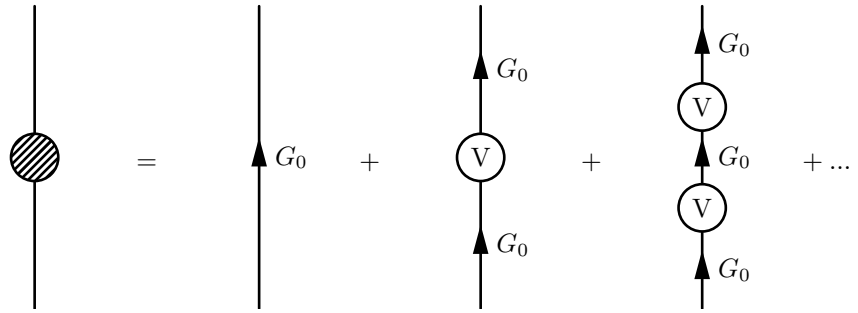

FIGURE 2.1: Diagram of Dysonśequation

amplitude for moving freely from y to x (free propagation G_0), added with the amplitude for propagation with a single scattering event at some point along the way G_0VG_0, added with the amplitude for propagation with two scatters $G_0VG_0VG_0$, and so on.

We can further process the expansion of G into geometric series of:

$$\begin{aligned} G &= G_0(1 + VG_0 + VG_0VG_0 + VG_0VG_0VG_0 + ...) \\ &= \frac{G_0}{1 - VG_0} \\ G &= \frac{1}{G_0^{-1} - V} \textbf{Dysonś} \text{ equation} \end{aligned}$$

We should notice that in Dysonśequation, we have sum of all perturbative term to infinity. So this equation is exact already (non-perturbative, non-approximative).

Several representation of the propagator can be identified by its domain as follows:

$$\begin{aligned} G_0^+(x, t_x, y, t_y) &= \text{ spacetime domain} \\ G_0^+(x, y, E) &= \text{ space and energy domain} \\ G_0^+(p, t_x, q, t_y) &= \text{ momentum and time domain} \\ G_0^+(p, E) &= \text{ momentum and energy domain} \end{aligned}$$

Universe is described as field combinations forming Lagrangian density $L[\phi(x)]$. Then we quantize these fields into a universe pictured as a vacuum that disturbed by field operators like $\hat{a}_p^\dagger$. The excitation of the vacuum that the fied operators produced are particles and antiparticles. How to keep track of these

particles? Using wave functions, we need some objects that contain the information about excitations of the system. These object are propagator amplitudes denoted by G. From here on, we have two theories, non-interacting and interacting theory. Non-interacting theories are those that can be diagonalized using canonical quantization, allowing us to describe the system in terms of a vacuum $|0\rangle$, and non-interacting particles in momentum states $|p\rangle$ created with operators like $\hat{a}_p^\dagger$. The Hamiltonian of non-interacting theory is called $\hat{\mathcal{H}}_0 = \sum_p E_p \hat{a}_p^\dagger \hat{a}_p$ and $\hat{H}_0 |p\rangle = E_p |p\rangle$. On the other hand, interacting theories cannot be diagonalized with canonical quantization. In interacting theories, the ground states would be $|\Omega\rangle$ with Hamiltonian $\hat{H}$. If we act on $|\Omega\rangle$ with operator $|\hat{a}_p^\dagger\rangle$, we would not necessarily get a state $|p\rangle$, we may get a superposition of many particles (whose momenta sum to p). Most of interacting field theories cannot be exactly solved, so we need to develop a perturbation process to make approximate calculations.

For interacting system in its ground state $|Omega\rangle$, we introduce an extra particle of our choice at a spacetime point (y^0, y) as a probe. This particle interacts with the system, possibly causing excitation in the fields and or any other complex fenomena. Then we remove (annihilate) the particle at spacetime point (x^0, x) and finally check wether the system has remained in the interacting ground state $|\Omega\rangle$. From this, we interested in the amplitude $G^+(x, y)$ known as probability amplitude that the system is still in its ground state after we create a particle at y and later annihilate it at x (emphasized by + sign, and guaranteed by θfunction on the right), given by:

$$G^+(x,y) = \langle\Omega| \left(\text{annihilated particle at } (x^0, x)\right) \left(\text{created particle at } (y^0, y)\right) |\Omega\rangle$$
$$G^+(x,y) = \theta(x^0 - y^0) \langle\Omega|\hat{\phi}(x)\hat{\phi}^\dagger(y)|\Omega\rangle$$

2.4 Feynman Propagator

instead of G^+ that missed information about antiparticle due to constrain by θ-function, Richard Feynman introduce a more general Propagator. To get this, we introduce Wick time-ordering symbol T, so the scalar fields are always arranged earliest on the right, latest on the left.

bosonic: commuting (2.116)

$$T\hat{\phi}(x^0)\hat{\phi}(y^0) = \begin{cases} \hat{\phi}(x^0)\hat{\phi}(y^0), & x^0 > y^0 \\ \hat{\phi}(y^0)\hat{\phi}(x^0), & x^0 < y^0 \end{cases} \tag{2.117}$$

fermionic: anti-commuting (2.118)

$$T\hat{\phi}(x^0)\hat{\phi}(y^0) = \begin{cases} \hat{\phi}(x^0)\hat{\phi}(y^0), & x^0 > y^0 \\ -\hat{\phi}(y^0)\hat{\phi}(x^0), & x^0 < y^0 \end{cases} \tag{2.119}$$

Feynman Propagator: (2.120)

$$G(x,y) = \langle\Omega|T\hat{\phi}(x)\hat{\phi}^\dagger(y)|\Omega\rangle \tag{2.121}$$

$$= \theta(x^0-y^0)\,\langle\Omega|T\hat{\phi}(x)\hat{\phi}^\dagger(y)|\Omega\rangle + \theta(y^0-x^0)\,\langle\Omega|T\hat{\phi}^\dagger(y)\hat{\phi}(x)|\Omega\rangle \tag{2.122}$$

Thus the total propagator have two parts, when initial time is y^0, first part creates a particle at y and propagates it to x and destroy it. the second part happens when initial time is x^0, it creates antiparticle at x and propagates it to y.

If the system have no interactions, then particles just move around passing through each other. We would call the ground state as $|0\rangle$, and we have *free propagator* $G_0(x,y)$ or $\Delta(x,y)$:

$$\Delta(x,y) = \langle 0|T\hat{\phi}(x)\hat{\phi}^\dagger(y)|0\rangle \tag{2.123}$$

$$= \int \frac{d^3p}{(2\pi)^3(2E_p)}\left[\theta(x^0-y^0)e^{-ip.(x-y)} + \theta(y^0-x^0)e^{ip.(x-y)}\right] \tag{2.124}$$

feynman diagram for particle + antiparticle = Feynman propagator

Δ symbolically depicted as a line without interaction blob since a free particle does not interact with any other particle on its way from y to x. In perturbation approach, essentially we see interactions as events that take place at particular spacetime points (i.e. V-blobs), and we imagine that the particles propagate freely between interactions with the free propagator. We get Feynman propagator from addition between particle part from retarded half of the propagator and antiparticle part from the advanced half of the propagator. For interacting case, these propagator is not truly Green's function. But, free-propagator functions are the Green's functions of the equation of motion. thus for scalar field we have:

$$(\partial^2 m^2)\Delta(x-y) = -i\delta^{(4)}(x-y) \tag{2.125}$$

In this scalar field theory, we need free Feynman propagator that have no step functions. We can have this by using complex analysis.

$$\Delta(x,y) = \langle 0|T\hat{\phi}(x)\hat{\phi}^{\dagger}(y)|0\rangle$$
$$= \int \frac{d^3p}{(2\pi)^3(2E_p)}\left[\theta(x^0-y^0)e^{-ip.(x-y)} + \theta(y^0-x^0)e^{ip.(x-y)}\right]$$

using: $\theta(x^0-y^0) = i\int_{-\infty}^{\infty}\frac{dz}{2\pi}\frac{e^{-iz(x^0-y^0)}}{z+i\varepsilon}$

the first term would become:

$$[\Delta(x_y)]_{(1)} = \theta(x^0-y^0)\int \frac{d^3p}{(2\pi)^3(2E_p)}e^{-iE_p(x^0-y^0)+ip.(x-y)}$$
$$= i\int_{-\infty}^{\infty}\frac{dzd^3p}{(2\pi)^4(2E_p)}\frac{e^{-i(E_p+z)(x^0-y^0)+ip.(x-y)}}{z+i\varepsilon}$$

substituting $z' = z + E_p$

$$[\Delta(x_y)]_{(1)} = i\int_{-\infty}^{\infty}\frac{dz'd^3p}{(2\pi)^4(2E_p)}\frac{e^{-iz'(x^0-y^0)+ip.(x-y)}}{z'-E_p+i\varepsilon}$$

we change the definition of four-momentum in integral,

treating z' as the new p^0 redefining $p = (z', p) = (p^0, p)$

$$[\Delta(x_y)]_{(1)} = i\int_{-\infty}^{\infty}\frac{d^4p}{(2\pi)^4(2E_p)}\frac{e^{-ip.(x-y)}}{p^0-E_p+i\varepsilon}$$

with this redefinition, $p^0 = E \neq (p^2+m^2)^{1/2}$, but $E_p = (p^2+m^2)^{1/2}$.

same process for second term, we have:

$$[\Delta(x_y)]_{(2)} = -i\int_{-\infty}^{\infty}\frac{d^4p}{(2\pi)^4(2E_p)}\frac{e^{-ip.(x-y)}}{p^0+E_p-i\varepsilon}$$

considering full propagator as sum of above two terms, we have:

$$\Delta(x_y) = [\Delta(x_y)]_{(1)} + [\Delta(x_y)]_{(2)}$$
$$= i\int_{-\infty}^{\infty}\frac{d^4p}{(2\pi)^4(2E_p)}e^{-ip.(x-y)}\left(\frac{1}{p^0-E_p+i\varepsilon} - \frac{1}{p^0+E_p-i\varepsilon}\right)$$
$$= \int_{-\infty}^{\infty}\frac{d^4p}{(2\pi)^4}e^{-ip.(x-y)}\left(\frac{i}{(p^0)^2-(E_p)^2+i\varepsilon}\right)$$

using $E_p^2 = p^2 + m^2$

$$\Delta(x_y) = \int_{-\infty}^{\infty}\frac{d^4p}{(2\pi)^4}e^{-ip.(x-y)}\frac{i}{(p^2-m^2+i\varepsilon)}$$: free Feynman propagator

with Fourier component corresponding to a particle with momentum p

$$\widetilde{\Delta}(p) = \frac{i}{(p^2-m^2+i\varepsilon}$$

Furthermore, Hideki Yukawa postulated that particles interact by exchanging virtual, force-carrying particles[20]. For a very small window of time, we are allowed to have a *virtual particle*, a particle that exist in "off mass-shell", where it can disobey mass-shell four-dimensional surface equation $p^2 = E_{\boldsymbol{p}}^2 - \boldsymbol{p}^2 = m^2$. By the constrain of $\Delta E \Delta t \ \hbar$, we can allow a particle of energy E to exist off the mass-shell as long as they last under duration of $\Delta t \simeq \hbar/E$. As a consequence, virtual particles must have finite range. Potential $U(\boldsymbol{r})$ mediated by the virtual particle can be expressed as:

$$U(\boldsymbol{r}) \propto -\frac{e^{-|\boldsymbol{r}|/a}}{4\pi|\boldsymbol{r}|} \tag{2.126}$$

Yukawa particle exchange process works as this. At a time y^0, particle A emits virtual particle Q with mass m_Q from position $\boldsymbol{y}$. At later time x^0, particle A collides with particle B at position $\boldsymbol{x}$. We take the energy of this process as $E_A = E'_A + E_Q$, meaning that particle A lost energy of $E_Q = (\boldsymbol{p}_Q^2 + m_Q^2)^{1/2}$, while particle B gains energy of E_Q. For the sake of symmetric energy transfer (not only from A to B), we construct additional process. Here, particle B at position $\boldsymbol{x}$ emits an identical virtual particle Q at time x^0 that collides with A at spacetime $(y^0, \boldsymbol{y})$. This process is already described by free Feynman propagator:

$$\Delta(x,y) = \theta(x^0 - y^0)\,\langle 0|T\hat{\phi}(x)\hat{\phi}^\dagger(y)|0\rangle + \theta(y^0 - x^0)\,\langle 0|T\hat{\phi}^\dagger(y)\hat{\phi}(x)|0\rangle$$
$$\widetilde{\Delta}(p) = \frac{i}{(p^2 - m^2 + i\varepsilon} = \frac{i}{((p^0)^2 - \boldsymbol{p}^2 - m^2 + i\varepsilon}$$

this expression is well behaved only when $p^0 \neq \sqrt{\boldsymbol{p}^2 + m^2}$, meaning that this equation is always off mass shell. It means the propagation of virtual particles are already described by the Green's function.

If we evaluate deeper in free propagator $\Delta(x,y)$ for scalar field theory, we have that the equation involves a singularity where $p^2 = E_{\boldsymbol{p}}^2 - \boldsymbol{p}^2 = m^2$. Here we include $i\varepsilon$ to ensure that the integral never hits this singularity.

To understand this $i\varepsilon$, we need to understand complex analysis. If a function is analytic in a region around point z, then it has a derivative at every point in that region. And this derivative should not depend on the way the interval in the complex plane Δz is selected. Derivative of a complex number defined as:

$$\frac{df}{dz} = \lim_{\Delta z \to 0} \frac{\Delta f(z + \Delta z) - f(z)}{\Delta z} \tag{2.127}$$

$f(z) = z^2$ is analytic while $g(z) = |z|^2$ is not analytic because in $g(z)$, using $\Delta z = i\Delta y$, we have different derivative with $\Delta z = \Delta x$.

A pole is a type of singularity (undefined mathematical object), like where we have $lim_{x->0}\, 1/x$. Let $f(z)$ be analytic between two circles C_1 and C_2. Why circles we may ask? Because this is complex plane, and the complex value always defined in two parts, thus circles. In the region between these two circles, we can write $f(z)$ as a Laurent series expanded around z_0.

$$f(z) = a_0 + a_1(z - z_0) + a_2(z - z_0)^2 + .. + \frac{b_1}{z - z_0} + \frac{b_2}{(z - z_0)^2} + ... \quad (2.128)$$

Expression with b is called the principal part. Then we can find and define: 1. If all b are zero, then $f(z_0)$ is analytic at $z = z_0$. 2. If all b after b_n are zero, then we have a pole of order n at $z = z_0$. if $n = 1$, it called *simple pole*. 3. b_1 is *residue* of $f(z)$ at $z = z_0$.

Non-relativistic, retarded, free-electron propagator $G_0^+(E) = \frac{i}{E - E_{\boldsymbol{p}} + i\varepsilon}$ has first order pole at $E_{\boldsymbol{p}} - i\varepsilon$.

Feynman propagator for the free scalar field have particle and antiparticle part. The particle part would have a simple pole at $p^0 = E_{\boldsymbol{p}} - i\varepsilon$ while the antiparticle have simple pole at $p^0 = -E_{\boldsymbol{p}} + i\varepsilon$.

Residue $R(z_0)$ at the pole z_0 can be found by examining the Laurent series. For a simple pole, we would have $R(z_0) = lim_{z->z_0}(z - z_0)f(z)$. In this breath, we have the residue of $G(E) = \frac{iZ}{E - E_{\boldsymbol{p}} + i\varepsilon}$ at simple pole $E_{\boldsymbol{p}} - i\varepsilon$ is iZ.

Back to general interacting theory $G(x, y) = \langle\Omega|\hat{\phi}(x)\hat{\phi}^\dagger(y)|\Omega\rangle$. $|\Omega\rangle$ is the interacting ground state. $G(x, y)$ is *single-particle propagator* or *two-point Green's function*. The diagram would be a shaded blob with two stumps extruded correspond to incoming and outgoing particles. The shaded blob is the interaction that experienced by our particle (creating and annihilation). "Two-point" means single particle created plus one particle annihilated. In another language, it can be written as $G^{(2)}$, $G(1, 2)$, etc. Our aim in quantum field theory is to find the full interacting Green's function $G^{(n)}$, because: 1. G can be used to calculate scattering amplitudes using LSZ reduction formula. 2. the form of the interacting G tells us a lot about the system.

From a free scalar theory, before interactions, we have free propagator $\widetilde{\Delta}(p) = \frac{i}{p^2 - m^2 + i\varepsilon}$. Mass of particle is given by the position of the pole ($m = \pm p$). The residue at the pole is i, means the operator $\hat{\phi}^\dagger(y)$ creates one quantum from the vacuum $|0\rangle$ that we destroy later at x. In interacting system, the full propagator is similiar with free propagator.

$$\widetilde{G}^2(p) = \frac{iZ_{\boldsymbol{p}}}{p - 2 - m^2 - \widetilde{\Sigma}(p) + i\Gamma_{\boldsymbol{p}}} + (M.terms) \tag{2.129}$$

1. $Z_{\boldsymbol{p}}$ the probability of stable particle with momentum $\boldsymbol{p}$ exist undestroyed by the interactions.
2. $\widetilde{\Sigma}(p)$ the interaction between particle with momentum p and the vacuum.
3. $(2\Gamma_{\boldsymbol{p}})^{-1}$ is the particleślifetime
4. M.terms hold the contribution from short-lived multiparticle states that can be exist out of the vacuum.

The Lagrangian describing the quantum fiewld usually consisted of a sum of solvable part (non-interacting particles, free part) and unsolvable part (describes interactions, thus interacting part). Free part can be solved via canonical quantization and resulted in non-interacting particles. Interaction part involve creation and destruction of particles. One example of interaction process is particle scattering. Here, particles are fired at each other. Initially, each particles are far away, assumed as non-interacting (free particle). Then, the smashed together for a very short time (interacting). This simple phenomena will be a basis for describing more general perturbation theory that deals with other interactions.

First building block of quantum field theory is the scattering or *S-matrix* of John Wheeler. First, we start with separated particles that run to each other. Then those particles interact with each other following Hamiltonian of the real world $\hat{H}$. Finally, those particles moving out of the interaction, and separated again into free particles.

Let us work in Heisenberg pictures. Wheeler start by assuming that the world is constructed as a sum of complicated interactions and non-interaction, meaning we split $\hat{H} = \hat{H}_0 + \hat{H}'$. $\hat{H}_0$ is for simple world of non-interacting particles described by some set of state vectors. In Heisenberg pictures, these state vectors are not changed. For two particles, we may take a momentum state of $|\psi\rangle = |p_2 p_1\rangle^{in}_{simple}$ as a simple-world state. Then we try to find a real-world state that looks like this simple-world state, and we found such state at the start of scattering. When the particles are very far apart, at time $(t- > -\infty)$, we have *in-state* of $|p_2 p1\rangle_{real}$. Then we take another simple-world state $|\phi\rangle = |q_2 q_1\rangle$. Once again, we found similiar real-world state at $t- > \infty$ when particles are separated after interaction. We have this real-world state as $|q_2 q_1\rangle^{out}_{real}$ Thus we have the simple-world states are only good for the real world in the limits $t- > \pm\infty$.

We are interested in the amplitude A that started with $|p_2 p_1\rangle^{in}_{real}$ and ended by $|q_2 q_1\rangle^{out}_{real}$.

$$A = {}^{out}_{real}\langle q_1 q_2 | p_2 p_1 \rangle^{in}_{real} \tag{2.130}$$

We recreate this amplitude using simple-world states using S-matrix, by defining:

$$A = {}^{out}_{real}\langle q_1 q_2 | p_2 p_1 \rangle^{in}_{real} = {}_{simple}\langle q_1 q_2 | \hat{S} | p_2 p_1 \rangle_{simple} \tag{2.131}$$

From this, we need two answer two questions: 1. How to get suitable $\hat{H}_0$ to describe some useful simple-world states that resemble in/out states. 2. How to calculate expression of $\hat{S}$, and use the eigenstates of the simple Hamiltonian to get an amplitude.

To get the answer for $\hat{H}_0$, we have interaction representation.

As previously stated, we separate $\hat{H} = \hat{H}_0 + \hat{H}'$, with $\hat{H}_0$ is free part and the other one is interaction part. Then we define operators in interaction picture $\hat{O}_I$ evolve in time via free part $\hat{H}_0$

$\hat{O}_I(t) = e^{i\hat{H}_0 t}\hat{O}e^{-i\hat{H}_0 t}$ just like Heisenberg mechanics using free part

$$i\frac{d\hat{O}_I}{dt} = \left[\hat{O}_I(t), \hat{H}_0\right]$$

We also compare a matrix element from Schrödinger picture to one in interaction picture:

$$\langle\phi(t)|\hat{O}|\psi(t)\rangle = \langle\phi_I(t)|e^{i\hat{H}_9 t}\hat{O}e^{-i\hat{H}_0 t}|\psi_I(t)\rangle$$

Thus, for the matrix elements to be the same as in the Schrödinger picture, we need:

$$|\psi_I(t)\rangle = e^{i\hat{H}_0 t}\,|\psi(t)\rangle$$

equation of motion for interaction picture will be:

$$\begin{aligned} i\frac{d}{dt}|\psi_I(t)\rangle &= e^{i\hat{H}_0 t}\left(-\hat{H}_0 + i\frac{d}{dt}\right)|\psi(t)\rangle \\ &= e^{i\hat{H}_0 t}\left(-\hat{H}_0 + \hat{H}\right)|\psi(t)\rangle \end{aligned}$$

$$\text{thus } i\frac{d}{dt}|\psi_I(t)\rangle = e^{i\hat{H}_0 t}\hat{H}'e^{-i\hat{H}_0 t}|\psi_I(t)\rangle$$

$$i\frac{d}{dt}|\psi_I(t)\rangle = \hat{H}_I(t)\,|\psi_I(t)\rangle \longleftarrow \hat{H}_I(t) = e^{i\hat{H}_0 t}\hat{H}'e^{-i\hat{H}_0 t}$$

In overall, interaction picture is described by:

1. The ability of operators and states to change in time.
2. The change of operators denoted by free part $\hat{\phi}_I(t) = e^{i\hat{H}_0 t}\hat{\phi}e^{-i\hat{H}_0 t}$
3. The change of states follows interaction part $i\frac{\partial}{\partial t}|\psi(t)\rangle_I = \hat{H}_I(t)|\psi_I(t)\rangle$ where $\hat{H}_I(t) = e^{i\hat{H}_0 t}\hat{H}'e^{-i\hat{H}_0 t}$.
4. All representations coincide at $t = 0$.

For an example, we can apply interaction picture to scattering experiment. Here, interaction picture of the beginning and the end of the experiments are simple-world states (non-interacting, free, bare vacuum $\hat{H}_0$ from $|0\rangle$). During interaction, $\hat{H}_I$ is nonzero. Considering operators, they will time-evolve according to $\hat{H}_0$. On the other hand, the states can be identified as eigenstates of $\hat{H}_0$, that generated from vacuum of $\hat{H}_0$ denoted as state $|0\rangle$. During interaction, we have non-zero $\hat{H}_I$, and the states evolves in any way it seem fit. However, at the end of the experiment, $\hat{H}_I$ is zero, and the state freeze. The last consideration is on $\hat{S}$-operator. By definition, all our quantum mechanical pictures in this model is defined in such a way that they would coincide at $t = 0$. It means we would have

$$_{simple}\langle\phi|\hat{S}|\psi\rangle_s \; imple =^{out}_{real} \langle\phi|\psi\rangle^{in}_{real} = \langle\phi_I(0)|\psi_I(0)\rangle$$

by using $\hat{U}(t_2, t_1)$ as the time-evolution operator in the interaction picture, we would have:

$$\begin{aligned} {}_{simple}\langle\phi|\hat{S}|\psi\rangle_{simple} &= \langle\phi(\infty)|\hat{U}_I(\infty, 0)\hat{U}_I(0, -\infty)|\psi(-\infty)\rangle \\ &=_{simple} \langle\phi|\hat{U}(\infty, -\infty)|\psi\rangle_{simple} \end{aligned}$$

This means, in this case, $\hat{S}$-operator is the time evolution operator for interaction-picture $\hat{U}(t, -t)$ as $t \to \infty$.

The perturbation expansion of S-matrix requires us to consider equation of motion for interaction picture time-evolution operator as in Equation 2.132.

$$i\frac{d}{dt_2}\hat{U}_I(t_2, t_1) = \hat{H}_I(t_2)\hat{U}_I(t_2, t_1) \text{ where } \hat{U}(t, t) = 1 \tag{2.132}$$

The solution of this motion is a time-ordered product $T[\hat{A}_1(t_1)\hat{A}_2(t_2)...\hat{A}_n(t_n)]$. This product is constructed by put the later operators on the left of the string of operators. Here, once again, we have Wickśtime ordering symbol $T[\ ]$ following the rules illustrated by equations **??**. As a result, we would have expression for

the time-evolution operator as follows:

$$\hat{U}_I(t_2,t_1) = T\left[e^{-i\int_{t_1}^{t_2} dt \hat{H}_I(t)}\right] \textbf{ Dyson's expansion}$$

or in its expanded form would be:

$$\hat{S} = T\left[1 - i\int d^4z \hat{H}_I(z) + \frac{(-i)^2}{2!}\int d^4y d^4w \hat{H}_I(y)\hat{H}_I(w) + ...\right]$$

The process to solve the vacuum expectation value $\langle 0|T[\hat{O}_1...\hat{Z}]|0\rangle$ of long time-ordered strings of operators, i.e. as pointed in Dysonśexpansion, is usually hard. On the other hand, its much easier to evaluate a normal-ordered strings as in $\langle 0|N[\hat{O}_1...\hat{Z}]|0\rangle$. The theorem to convert time-ordered into a normal-ordered form shown by following formula:

$$T[\hat{A}\hat{B}\hat{C}...\hat{Z}] = N\left[\hat{A}\hat{B}\hat{C}...\hat{Z} + \begin{matrix}\text{all possible contractions of} \\ \hat{A}\hat{B}\hat{C}...\hat{Z}\end{matrix}\right]$$

At this point, we may be overwhelmed by the sheer amount of symbols and notations presented in the mathematical formula mentioned so far. These densely packed mathematical formula, may reduce our capability to grasp some pattern that may arise from those equations. Richard Feynman have acknowledged this problem, and invented a "language" that represent the same above formulas more concisely as Feynman Diagrams. This language utilizes a set of shapes, i.e. vertices, wiggly lines, blob, etc. and imposes some rules to enable a translation back and forth to a mathematical formula. On the specification of Feynman diagrams, we identify some common shapes of vertices according to Table **??**. As a rule, usually we use vertical axis as a representation of time-axis, and horizontal axis as a representation of space-axis. We should keep in mind that space-axis may consisted of 3-degree of freedom. The interaction would be represented vertices or dot in the diagram, and the story of the particles flows in timely manner.

2.5 GW Approximation

In this approximation, let us consider an excitation of a single electron (producing a hole) by a photon. We may illustrate this process as a transition from a space-time coordinate $x \equiv (\mathrm{r}, \mathrm{t})$ to another space-time coordinate x'. In this illustration, our focus is in time of t and t'. For $t > t'$, we would see the Green's function as a probability amplitude of an electron added at x' will propagate to x. Whileas for $t' > t$, we see it as a probability amplitude of a hole created at x

will propagate to x'. Following the the property and possible stories of Green's function at **??**, we may reconstruct the definition of G into:

$$iG(x,x') = \langle N|T[\psi(x)\psi^\dagger(x')]|N\rangle \tag{2.133}$$

$$= \begin{cases} \langle N|T[\psi(x)\psi^\dagger(x')]|N\rangle \text{ for electron}, & t > t' \\ \langle N|T[\psi^\dagger(x')\psi(x)]|N\rangle \text{ for hole}, & t' > t \end{cases} \tag{2.134}$$

In equation **??**, we denoted the ground state of N electrons as $|N\rangle$, and we have time ordering operator already described for fermionic system in **??**. We also recall that the Green function actually is just another mathematical representation of particle (in this case, electrons), in the same theme as wave-functions that have already gains some initial popularity in Schrödinger construction. In such case, we can expect some quantities that can be acquired from Green function, namely:

1. Expectation value of single-particle operator in the ground state
2. The ground state energy
3. The excitation spectrum.

The single-particle Green function of **??** would be used as a base for our further explanation on Hedin's formulation.

2.6 Green Function in Heisenberg representation

We use Heisenberg representation to connect the Green function with the self-energy. In this representation, we ought to satisfy the equation of motion following:

$$\begin{aligned} i\frac{\delta}{\delta t}\psi(x) &= [\psi(x), \hat{\mathcal{H}}] = \psi(x)\hat{\mathcal{H}} - \hat{\mathcal{H}}\psi(x) \\ \hat{\mathcal{H}} &= \int dx\ \psi^\dagger(x)h_0(x)\psi(x) \\ &\quad + \frac{1}{2}\int dx\ dx'\ \psi^\dagger(x)\psi^\dagger(x')v(x-x')\psi(x')\psi(x) \\ v(x-x') &= v(|r-r'|)\delta(t-t') \end{aligned}$$

In this equation, we have h_0 represents kinetic energy and any local external field. From the commutator $[\psi(x), \widehat{\mathcal{H}}]$, we get the equation of motion for the Green function as follows:

$$\delta(x-x') = \left[i\frac{\delta}{\delta t}\psi(x) - h_0(x)\right] G(x,x') + i\int d^3r_1\ (r-r_1)\,\langle N|T[\psi^\dagger(r_1,t)\psi(r,t)\psi(r,t)\psi^\dagger(r',t')]|N\rangle \quad (2.135)$$

The braket at the right hand side of equation **??** can be viewed as a two-particle Green function. This two-particle Green function generally represented as

$$G_2(x_1,x_2,x_3,x_4) = i^2\,\langle N|T[\psi(x_1)\psi(x_3)\psi^\dagger(x_4)\psi^\dagger(x_2)]|N\rangle$$

for propagation of two particles from x_2, x_4 to x_1, x_3 respectively. Thus, interestingly, we realized that the single particle Green function would be generated from two-particle Green function. And furthermore, the two-particle Green function from three-particle Green function, and so on. This scheme recursively generates a chain of equations that spans infinitely.

This chained equations can be broken by introducing *the mass operator M* that can be constructed as:

$$\int dx_1\ M(x,x_1)G(x_1,x') = -i\int d^3r_1\ (r-r_1)\,\langle N|T[\psi^\dagger(r_1,t)\psi(r,t)\psi(r,t)\psi^\dagger(r',t')]|N\rangle \quad (2.136)$$

In such a way, we can substitute **??** into **??** and get a non-recursive form of:

$$\delta(x-x') = \left[i\frac{\delta}{\delta t}\psi(x) - h_0(x)\right] G(x,x') - \int dx_1\ M(x,x_1)G(x_1,x') \quad (2.137)$$

In this construction, we can see that M introduce the components of hartree and self-energy.

In a first principle calculation, the self-energy of finite system such as a molecule can be done using a finite order perturbation theory. On the other hand, for extended system (crystal, surfaces, etc.) the issue is quite harder, due to the long-range nature of Coulomb interaction. This called for infinite

expansion of the perturbation series to achieve a physically sensible results. However, the mechanism of expansion tends to be done by physical intuition and quite peculiar in case by case basis.

2.7 Green Function in Dirac representation

One method to evaluate the perturbation expansion of self-energy is by the functional derivative technique introduced by Hedin[21]. We use Dirac representation as a starting point of this evaluation. As a mathematical tools, we would use a time varying field $\pi(r,t)$ that will be zeroed out in the final step, once we procure self-energy. In Dirac picture, we would have:

$$|\psi_D(r,t)\rangle = \hat{U}(t,t_0)\,|\psi_D(r,t_0)\rangle \tag{2.138}$$

as we have time development operator $\hat{U}$ is represented by:

$$\hat{U}(t,t_0) = Texp\left[-i\int_{t_0}^{t} d\tau\ \pi(\tau)\right]\ \pi(t) = \int d^3r\ \pi(r,t)\psi_D^{\dagger}(r,t)\psi_D(r,t) \tag{2.139}$$

we can connect Dirac and Heisenberg pictures by considering Dirac picture as an unperturbed ($\pi = 0$) Heisenberg, using:

$$\psi(x) = \hat{U}^{\dagger}(t,0)\psi_D(x)\hat{U}(t,0)i\frac{\partial}{\partial t}\psi_D(x) = [\psi_D(x), \hat{H}(\pi = 0)] \tag{2.140}$$

In this case, we would have Green function in Dirac picture as:

$$iG(1,2) = \frac{\langle N^0|T[S\psi_D(1)\psi^{\dagger}(2)]|N^0\rangle}{\langle N^0|T[S|N^0\rangle} \tag{2.141}$$

and for two-particle Green function, we would have:

$$G_2(1,2,3,4) = (i)^2\frac{\langle N^0|T[S\psi_D(1)\psi_D(3)\psi_D^{\dagger}(4)\psi^{\dagger}(2)]|N^0\rangle}{\langle N^0|T[S|N^0\rangle} \tag{2.142}$$

in which $S = U(\infty, -\infty)$ and the unperturbed ground state (interacting groundstate with $\pi = 0$) is denoted by $|N^0\rangle$.

Using these definitions, we can proceed to a functional form of S:

$$S = U(\infty, -\infty) = Texp[-i \int_{-\infty}^{\infty} d\tau \ \pi(\tau)]$$
$$S = Texp[-i \int_{-\infty}^{\infty} d\tau \int 3r \ \pi(r,t)\psi_D^\dagger(r,t)\psi_D(r,t)]$$
$$S[\pi] = Texp[-i \int d\tau\pi(\tau)\psi_D^\dagger(r,t)\psi_D(r,t)]]$$

The functional derivative of S respective to π can be achieved by having $\frac{\delta S}{\delta \pi}$ conforms:

$$\int dr \ \frac{\delta S}{\delta\pi(3)}\varphi(3) = \left[\frac{d}{d\epsilon}S[\pi + \epsilon\varphi]\right]_{\epsilon=0}$$
$$\int dr \ \frac{\delta S}{\delta\pi(3)}\varphi(3) = \int dr \ T[S\psi_D^\dagger(3)\psi_D(3)]\varphi(3)$$
$$\frac{\delta S}{\delta\pi(3)} = T[S\psi_D^\dagger(3)\psi_D(3)]$$

And following the functional derivative of single-particle Green function would be:

$$\frac{\delta G(1,2)}{\delta\pi(3)} = G(1,2)G(3,3^+) - G_2(1,2,3,3^+)$$

Combining these results with the general form of self-energy and hartree M that we already have at **??**, we would have:

$$\int d3 \ M(1,3)G(3,2) = \int d2 \ v(1-2)\rho(2)G(1,2) + i\int d3 \ v(1,3)\frac{\delta G(1,2)}{\delta\pi(3)} \tag{2.143}$$
$$?? < -V_H(1) \tag{2.144}$$

In this stage, we may define the self-energy Σ as:

$$\Sigma = M - V_H \tag{2.145}$$

and by taking leverages on the identity of:

$$\frac{\delta}{\delta\pi}(G^{-1}G) = 0 \text{ and } \frac{\delta G}{\delta\pi} = -G\frac{G^{-1}}{G}G \tag{2.146}$$

we can get the rough form of Σ following:

$$\Sigma(1,2) = -i\int d3\ d4\ v(1,4)G(1,3)\frac{\delta G^{-1}(3,2)}{\delta\pi(4)} \tag{2.147}$$

$$= -i\int d3\ d4\ v(1,4)G(1,3)\frac{\delta G^{-1}(3,2)}{\delta V(5)}\frac{\delta V(5)}{\delta\pi(4)}\ d5 \tag{2.148}$$

$$\text{with } V = V_H + \pi \tag{2.149}$$

We can further simplify the formulation of Σ by taking some physical definition on several parts of **??**:

$$\Sigma(1,2) = i\int d3\ d4\ G(1,3)d5\ v(1,4)\underbrace{\frac{\delta V(5)}{\delta\pi(4)}}_{\epsilon^{-1}(1,2)}\underbrace{(-\frac{\delta G^{-1}(3,2)}{\delta V(5)})}_{\Lambda(1,2,3)} \tag{2.150}$$

$$W(1,2) = \int d3\ v(1,3)\epsilon^{-1}(2,3) \tag{2.151}$$

In these parts, we have W as a screened version of Coulomb interaction $v(1,3)$ by inverse of dielectric function ϵ^{-1}. We also define Λ as the vertex function, that we should expand later. Finally, we would have the simplified form of Σ as :

$$\Sigma(1,2) = i\int d3\ d4\ G(1,3)\ W(1,4)\ \Lambda(3,2,4) \tag{2.152}$$

In case of vertex function Λ, we can write it as:

$$\begin{aligned}\Lambda(1,2,3) &= -\frac{\delta G^{-1}(1,2)}{\delta V(3)} \\ &= \delta(1-2)\delta(2-3) + \frac{\delta\Sigma(1,2)}{\delta V(3)} \\ &= \delta(1-2)\delta(2-3) + \int d(4,5,6,7)\ \frac{\delta\Sigma(1,2)}{\delta G(4,5)}G(4,6)G(7,5)\Lambda(6,7,3)\end{aligned} \tag{2.153}$$

Interestingly, the formulation of vertex function actually give us a recursive function. There are several ways to address this vertex function, much or less by simplification either by assumption or by truncation. Nonetheless, by now, we have addressed several important concepts of Hedin formula, namely G, Σ, W, and Λ.

2.8 The Polarization function Π

Derived from the inverse dielectric function, we can arrange:

$$
\begin{aligned}
V_H(1) &= \int d2\ v(1-2)\rho(2)...?? \\
V &= V_H + \pi...?? \\
\epsilon^{-1}(1,2) &= \frac{\delta V(1)}{\delta \pi(2)}...?? \\
&= \frac{\delta}{\delta \pi(2)}(\pi(2) + V_H(1)) \\
&= \frac{\delta}{\delta \pi(2)}(\pi(2) + \int d3\ v(1-3)\rho(3)) \\
&= \frac{\delta \pi(2)}{\delta(\pi(2))} + \frac{\delta}{\delta \pi(2)}\left[\int d3\ v(1-3)\rho(3)\right] \\
&= 1 + v(1-2)\underbrace{\frac{\delta \rho(1)}{\delta \pi(2)}}_{\chi_(1,2)} \\
&= 1 + v(1-2)\underbrace{\frac{\delta \rho(1)}{\delta V(3)}}_{\Pi(1,3)}\frac{\delta V(3)}{\delta \pi(2)}
\end{aligned}
$$

The last two expression would develop our definition on polarization function Π and response function χ. In this definition, the response function χ is a change in the density with respect to the *external* potential π. On the other hand, the polarization function Π is that change with respect to the *total* potential V. We also should notice that at the last expression, we have once again a recursive function for $\epsilon - -1$ as a function of $\frac{\delta V}{\delta \pi}$ as described in **??**. We may further realize that while actually $\rho(1) = -iG(1,1^+)$, using identity **??** we can expand the polarization function Π into:

$$\Pi(1,2) = -i\int 3\ d4\ G(1,3)\Lambda(3,4,2)G(4,1^+) \tag{2.154}$$

At this point, we got the description of response function Π, and its connection with G and Λ. Using our new realization for Π, we may reconstruct our definition on W in **??**, and obtain:

$$\begin{aligned} W(1,2) &= \int d3\ v(1,3)\epsilon^{-1}(2,3) \\ &= \int d3\ v(1,3)\left[1 + v(3,4)\frac{\delta\rho(3)}{\delta V(4)}\frac{\delta V(4)}{\delta\pi(3)}\right] \\ W(1,2) &= v(1,2) + \int d3\ d4\ v(1,3)\Pi(3,4)W(4,2) \end{aligned}$$

In this final form, we have W as a recursive functional that needs polarization function Π in its calculation. At previous explanations, we have established the equation for Σ as a function of $G, W,$ and Λ. We also have described similiar relations for Λ. To complete our image on this equation system, we should explore the connection between G and Σ.

2.9 Connection between G and Σ

To establish the relation between G and Σ, we need a Fourier transformation of equation **??**:

$$[\omega - H_0(r)]G(r,r',\omega) - \int dr_1\ \Sigma(r,r_1,\omega)G(r_1,r',\omega) = \delta(r-r') \tag{2.155}$$

Therefore, the definition of quasiparticle wave-function Ψ_{qp} with energy E_{qp} is fulfilled by:

$$H_0(r)\Psi_{qp}(r,E) + \int dr_1\ \Sigma(r,r_1,\omega)\Psi_{qp}(r_1,E) = E_{qp}\Psi_{qp}(r,E) \tag{2.156}$$

By definition, the 0^{th} order Green function is described as:

$$\left[i\frac{\partial}{\partial t} - H_0(x)\right]G_0(x,x') = \delta(x-x') \tag{2.157}$$

Combining these definitions, we would have Dyson equation as follows:

$$G(x,x') = G_0(x,x') + \int dx_1\ dx_2\ G_0(x,x_1)\ \Sigma(x_1,x_2)\ G(x_2,x') \tag{2.158}$$

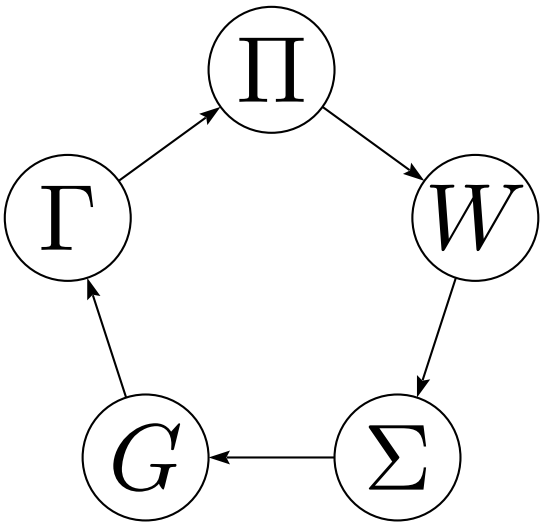

FIGURE 2.2: Simplified diagram of Hedin equations

equally in matrix form, we have $G = G_0 + G_0\Sigma G \leftrightarrow G^{-1} = G_0^{-1} - \Sigma$. In such way, we have the connection between G and Σ.

2.10 The Hedin equation

As a summary, we have described the Hedin equations and gains five important components, namely:

$$\Sigma(1,2) = i\int d(34)G(1,3^+)W(1,4)\Gamma(3,2,4) \tag{2.159}$$

$$G(1,2) = G^0(1,2) + \int d(34)G^0(1,3)\Sigma(3,4)G(4,2) \tag{2.160}$$

$$\Pi(1,2) = -i\int d3d4\Gamma(3,4,2)G(1,3)G(4,1^+) \tag{2.161}$$

$$W(1,2) = v(1,2) + \int d(34)v(1,3)\Pi(3,4)W(4,2) \tag{2.162}$$

$$\Lambda(1,2,3) = \delta(1-2)\delta(2-3) \tag{2.163}$$

$$+ \int d(4567)\frac{\delta\Sigma(1,2)}{\delta G(4,5)}G(4,6)G(7,5)\Gamma(6,7,3) \tag{2.164}$$

These equations can be simplified into a diagram shown in Figure **??**.

Just following these equations, we should be able to do an iterative calculation to get a satisfying Green function. However, we already shown that there are some recursive function appear in this construction. This called for an approximative treatment that we will consider later on.

2.11 GW Approximation

One simple approximation that we can do on Hedin equation, is by assuming the functions of $G = G_0$ and $\Sigma = 0$ in the formulation of vertex function Λ. This treatment would simplify the form of vertex function into:

$$\Lambda(1,2,3) = \qquad\qquad \delta(1-2)\delta(2-3)$$

This would further simplify the construction of Σ into:

$$\begin{aligned}\Sigma(1,2) &= i\int d(34)G(1,3^+)W(1,4)\Gamma(3,2,4)\\ \Sigma(1,2) &= i\int d(34)G(1,3^+)W(1,4)\end{aligned} \tag{2.165}$$

This form of $\Sigma = iGW$ is the root of the name "GW Approximation". Furthermore, this Σ is used as a basis for the calculation of all other equations in Hedin equations. Practically, in GW approximation, we consider G^0 as an input, and have Σ and eigenvalues ε_i as a raw converged output. We may generate G^0 input from a converged DFT results. Following a converged calculation of DFT resulting eigenvalues ε_i and eigenfunctions $\Psi_i(r)$, we can construct the non-interacting Green function by:

$$G^0(r,r',\omega) = \sum_j \frac{\Psi_j(r)\Psi_j^*(r')}{\omega - \varepsilon_j \mp i\delta}$$

In this construction, we denote $-i\delta$ for occupied states, and $+i\delta$ for unoccupied states. Then, we would follow the calculation cycle described in figure **??**, iteratively until we have a convergence.

The merits of GW approximation is quite well known, i.e.:

- In case of atoms, GW Approximation results are similiar with Hartree-Fock Approximation. This is due to the small screening effect that occured in the system. However, the polarization function still improve the HF results.
- GW Approximation improve the Hartree-Fock band energy gaps (reduce the HF gap).
- GW Approximation improve the DFT band energy gaps (enlarge the DFT gap).

A review study on the performance of GW Approximation on many large band gap semiconductors is shown in Figure **??**[11]. In this figure, we can see stark improvement of GW Approximation compared to DFT results. Despite of its merits, the GW Approximation have a sensitivity on its input wave-functions. It means, the different input wave-functions would produce the different results. This is quite problematic for a predictive investigation. In light of this problem, Kotani et.al proposed an improvement, well known as quasi-particle self-consistent GW method (QSGW).

2.12 Quasi-particle Self-consistent GW method

As an improvement of GW Approximation, QSGW adopts some assumption held by GWA, namely on describing the self-energy Σ and its relation with the description of vertex function Λ. However, there are some concepts that introduced by QSGW that do not exist in GWA. Some of those concepts are the use of quasi-particle, and the utilization of DFT construct inside the iterative cycle.

We use the description of quasi-particle wave-function described previously in **??**. Following Landau picture of quasi-particle, there should be one-particle-like excitations (quasiparticles), at least around Fermi level E_F, that comply:

$$\left[\frac{-\nabla^2}{2m} + V^{ext} + V^H + Re[\Sigma(E_i)] - E_i\right] |\Phi_i\rangle \ = 0 \tag{2.166}$$

for quasiparticle eigen functions and quasiparticle energies { _i(r),E_i}. In this equation, Re[X] denotes the Hermitian part of X as such that E_i is real for $\Sigma(E_i)$. Around E_F, anti-Hermitian part of $\Sigma(E_i)$ gets nearer to zero as $E_i \to E_F$. Thus we have describe "dressed quasiparticle". On the otherhand, we also have one-particle picture from $H^0 = \frac{-\nabla^2}{2m} + V^{eff}(r, r')$ that corresponds to eigenfunctions and quasi-particle energies $\varepsilon_i, \Psi_i(r)$. This is a description of "bare quasiparticle".

The bare quasiparticle interact with each other via the bare Coulomb interaction. The bare quasiparticle with H^0 would evolve to become dressed quasiparticle when the interaction with total Hamiltonian $\hat{H} - \hat{H}^0$ is turned on adiabatically. In this case, we can see the dressed quasiparticle as a bare quasiparticle that accompanied by an indused polarization cloud consisting of other bare quasiparticle, just like in GW Approximation.

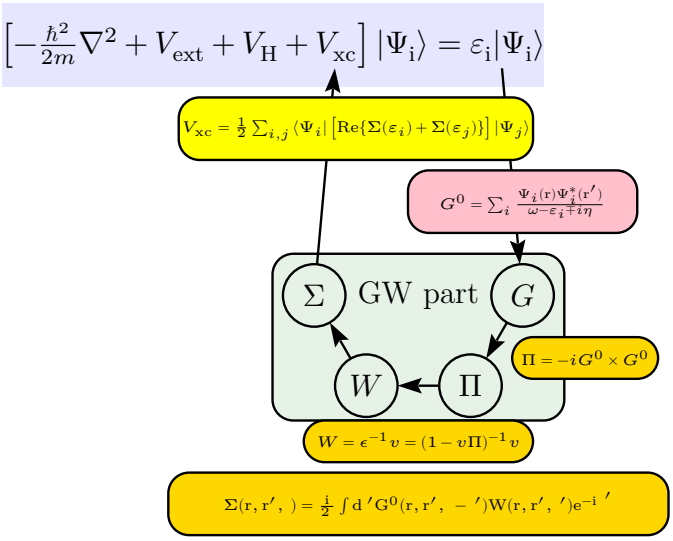

FIGURE 2.3: Schematic of self-consistent QSGW Method

In case of a self-consistent condition, we would have $\Psi_i, \varepsilon_i \approx \Phi_i, E_i$ around E_F. We already Ψ_i as a complete set due to H^0 origin, in contrast with Φ_i that is not a complete set. In this case, we can expand $\text{Re}[\Sigma(\varepsilon_i)]\,|\Psi_i\rangle$ into:

$$\text{Re}[\Sigma(\varepsilon_i)]\,|\Psi_i\rangle = \sum_{j,i} |\Psi_j\rangle\,\text{Re}[\Sigma(\varepsilon_i)]_{ji}$$

with using $\text{Re}[\Sigma(\omega)]_{ij} = \langle\Psi_i|\text{Re}\Sigma(\omega)|\Psi_j\rangle$. Next, from this expression, we would define an energy-independent operator R as:

$$R = \sum_{j,i} |\Psi_j\rangle\ \ \text{Re}[\Sigma(\epsilon_i)]_{ji}\ \ \langle\Psi_i|$$
$$R\,|\Psi_i\rangle = \text{Re}[\Sigma(\epsilon_i)]\,|\Psi_i\rangle$$

In this case, we substitute $\text{Re}[\Sigma(E_i)]$ in equation **??**. Due to the nature of R that is not Hermitian, we ought to take the Hermitian part of R. Therefore, we can do the calculation of Φ_i, E_i from Ψ_i, ε_i, using:

$$V^{xc} = \text{Re}[R]$$
$$V^{xc} = \frac{1}{2}\sum_{ij} |\Psi_i\rangle\,\text{Re}[\Sigma(\varepsilon_i)]_{ij} + \text{Re}[\Sigma(\varepsilon_j)]_{ij}\,\langle\Psi_j|$$

At this point, we have a cycle of calculation from $V^{eff} \to V^{GW}(\omega) \to V^{eff}$.

The overall cycle of calculation, involving GW part and DFT part, is shown in diagram **??**. If we do single pass in this cycle, then we have a new band structure coming from one time update of V_{xc}. This approach well-known as One-shot QSGW Method. Self-consistent QSGW method is achieved by continuing the iteration of self-energy calculation and exchange-correlation function update. Due to complexity on total energy calculation, we do not rely the convergence criteria on total energy. Instead, we consider our system to be converged when we have relatively unchanged band structure, especially around our point of interest, i.e. Fermi level.

Chapter 3

Results and Discussion

3.1 $NiCo_2O_4$

3.1.1 Electronic structure

The energy band dispersions of inverse B are shown in Figures 3.1. These figures are results for GGA, one-shot GW, and QSGW methods. In general, there are several features revealed from these energy bands. All calculations revealed half-metallic properties of $NiCo_2O_4$, where an energy gap opens at the Fermi energy in the majority spin state. For the minority spin state two bands accross to the Fermi level in QSGW, whileas three bands in GGA and one-shot GW.

As shown in Figures 3.1, the valence band around the Fermi level consists of the three parts of oxygen orbital and two cation 3d orbitals. The oxygen part is separated from the cation parts with an energy gap, and in the majority spin state of GGA the cation parts are further separated to the occupied and unoccupied states below and above the Fermi level, respectively. In the one-shot GW, the cation part is separated to three parts in both of the majority and minority spin states. However, during the self-consisitent calculation of QSGW, the cation part {once} separated at the one-shot GW is merged partially. As a whole property, the band width of cation bands becomes narrow from GGA to QSGW.

Valence band of $NiCo_2O_4$ extends over different range of energy, depends on the methods. For majority spin, the band structure shown non-metallic property. GGA shown the largest band width of 2.4 eV. QSGW method resulted in about 2.1 eV band width, while One-shot QSGW gave the smallest band width of 1.9 eV. GGA, one-shot and full QSGW methods shown separation of valence bands into two smaller bands, separated by 0.4, 1.0 eV and 0.2eV respectively. The band width of the these sub-bands are greater in GGA methods, compared to the others. The upper sub-band (near Fermi level) of QSGW method shown no further separation, in contrast with one-shot QSGW and GGA results.

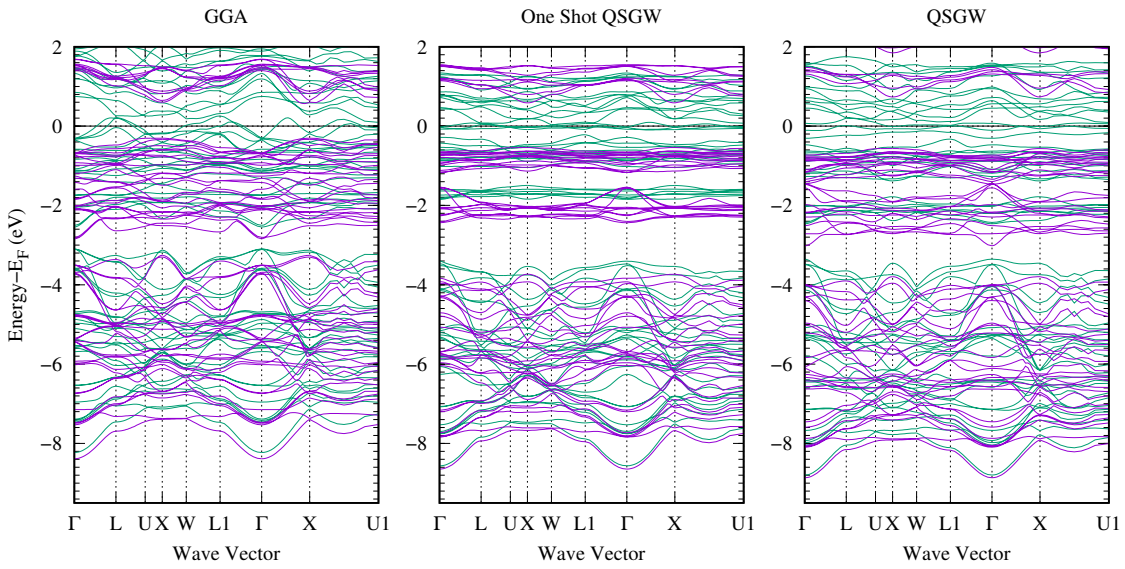

FIGURE 3.1: The energy band dispersions for $NiCo_2O_4$ with the inverse spinel type-B structure , green indicates minority spin states and magenta for majority ones. From left to right, the results of GGA, one-shot QSGW, and QSGW. The Fermi level presented by horizontal line is set at zero energy.

QSGW method produced semiconducting properties of majority spin of NiCo2O4 with bandgap of 1.02 eV and 1.15 eV for normal spinel structure and inverse spinel structure respectively.

Total and projected density of states (PDOS) obtained from GGA, one-shot GW, and QSGW are shown in Figures 3.2. All of PDOS display metallic behaviour only at the minority spin state. The cation band around the Fermi level is distributed, as if supposing the crystal field of octahedral or tetrahedral site. Such crystal field induces the energy splitting between t_{2g} and e_g states. The DOS shape of cation part becomes sharper from the result of GGA to those of one-shot GW and QSGW. In these GW results, the crystal field effect appears more clearly than those of GGA. This may be caused by the Coulomb interaction affected from O is taken into account more accurately through the screened Coulomb interaction W. Such effect may vary depending on the symmetry (octahedral or tetrahedral) of cation site. The sharp PDOS of cation bands may be due to a localization of electron wave functions for the transition metals. This feature is a typical consequence resulting from the GWA. Another consequence appearing in Figures 3.2 is observed on the oxygen band. That band is shifted to a lower energy, implying a stabilization on oxygen band in GWA.

The half-metallicity in the present work is in agreement with the previous theoretical results including the mBJ-LDA [8] and the LDA+U approaches[2, 5]. Overall DOS from the QSGW is similar to those from the mBJ-LDA and

LDA+U, whereas in the later, oxygen band is not separated from the cation band. In regards of cation band, the upper cation bands are shifted to the higher energies compared with the previous works mentioned above. The DOS of minority spin in vicinity of the Fermi level is overall similar to those in the previous works, but is different from them on quantitative detail. The orbital components will be discussed in the later part.

We note some features during the self-consisent iterative cycle by comparing the PDOS between one-shot GW and QSGW. First, the degree of energy splitting from crystal field increases in the self-consistent process. Second, as a result, the sharpness of DOS in one-shot GW becomes broaden, but have never reached to a broadness of DOS like GGA.

Figure 3.3 reported the total DOS and PDOS of normal spinel and inverse spinel (type A). As described before, half-metallic structure is observed. The energy level splitting caused by the crystal field is observed like those of the inverse spinel (type B), while the Ni(tet) component is missing in the latter case. An important difference against the inverse type B is a behavior at the Fermi level, as shown in Figure 3.4. Different with the case of inverse type B, the Fermi level crosses a large peak of DOS. These behaviors strongly imply that such metallic system have a possibility to take some form of instability. In other words, the electronic state can be stabilized further by some induction like a picture of Jahn-Teller effect. In the view of instability, the normal spinel or inverse type A may be at a higher energy state compared with the inverse type B.

3.1.2 Magnetic configuration

All of the methods (GGA, one-shot GW, and QSGW) provide a net magnetization of 2 μ_B/f.u. (f.u.: formula unit.) in the inverse spinel structures of type A and type B, and also normal spinel structure. This value of net magnetization has been reported in the previous works [4]. Both inverse structures provide a ferrimagnetic arrangement, whereas the normal spinel structure exhibits ferromagnetic arrangement. However, the ferrimagnetic arrangement provided by the inverse type A has a significant difference with that of type B. This is due to the difference of cation configuration between the inverse type A and type B.

Our total magnetization is much larger than the experimental value (1.25 μ_B/f.u.) [6]. Recent experiment [2] reported that the total magnetization gradually increases to a larger value (1.84 μ_B/f.u.) as the annealing time of specimen

increases. This difference on the magnetization may be attributed to a disordered crystal structure in experimental specimen.

Magnetic moment on each atom varied from GGA to QSGW, as shown in Table 3.1. The ferrimagetic configuration of inverse Type B is clearly indicated. The QSGW consistently shows a larger absolute value for each atomic magnetic moment except for Co(oct). This behavior can be understood since the QSGW tends to indicate more localized electronic state in d-orbital states. In the results of QSGW, the atomic magnetic moments of inverse B are 2.77 μ_B for Co(tet) and $-$1.39 μ_B for Ni. These results are comparable with the experimental data of Co(tet) 2.18 and Ni $-$1.49 μ_B [22] and the theoretical LDA+U data of 2.39 μ_B for Co(tet) and $-$1.12 μ_B for Ni [23] with U_{eff} [Ni, Co(tet) and Co(oct): 6.6, 4.7, and 6.7 eV, respectively, determined from a first-principles linear responce theory]. One of the interesting results is induction of non-negligible magnetic moment on O 2p orbitals. This contribution is estimated to be 0.40 μ_B in formula unit, resulting from the hybridization between cation 3d and O 2p orbitals. The occurence of magnetic moment on O atoms implies importance of its roles for understanding the electronic structure in $NiCo_2O_4$. The moment of Co(oct) indicates a small value, which coresponds a low spin state of Co atom.

In Table 3.2, magnetic moments of normal and inverse type A are reported. The ferromagnetic and ferrimagnetic configurations are indicated respectively. The moment of Ni(tet) is coupled ferromagnetically with those of Co(tet), while that of Ni(oct) is coupled antiferromagnetically. In all of the spinels investigated, the tetrahedral cation always contributes to ferromagnetic component, while the octahedral cation contributes to nonmagnetic or antiferromagnetic component. Additionally, the oxygen, even though the degree is small, contributes to ferromagnetic component. Interestingly, the sum of atomic components is commonly similar among the spinel structures investigated.

TABLE 3.1: Atomic and total magnetic moments (μ_B) in $NiCo_2O_4$ (inverse type B) from GGA, one-shot GW, and QSGW. Note that the averaged value is presented at O 2p.

Atom	GGA	one-shot GW	QSGW
Co(tet) 3d	2.34	2.77	2.77
Ni(oct) 3d	−0.87	−1.27	−1.39
Co(oct) 3d	0.09	0.02	0.07
O 2p	0.07	0.09	0.10
Sum in f.u.	1.81	1.86	1.86
Total in f.u.	2.00	2.00	2.00

TABLE 3.2: Atomic and total magnetic moments (μ_B) in the normal and inverse A spinels of $NiCo_2O_4$ from QSGW. Note that the averaged value is presented at O 2p.

Atom	Normal	Inverse A
Co(tet) 3d	-	2.76
Ni(tet) 3d	1.56	1.56
Ni(oct) 3d	-	−1.31
Co(oct) 3d	0.00	0.03
O 2p	0.09	0.08
Sum in f.u.	1.92	1.86
Total in f.u.	2.00	2.00

TABLE 3.3: Number of electrons in the projected orbitals in $NiCo_2O_4$ (inverse type B) from GGA, one-shot GW, and QSGW. u+d specifies the sum of up and down electrons.

Atom	GGA			one-shot GW			QSGW		
	up	down	u+d	up	down	u+d	up	down	u+d
Co(tet) 3d	4.56	2.22	6.77	4.67	1.89	6.56	4.66	1.89	6.55
Ni 3d	3.37	4.25	7.62	3.13	4.40	7.52	3.08	4.46	7.54
Co 3d	3.46	3.38	6.84	3.36	3.34	6.70	3.38	3.31	6.69
O 2p	1.74	1.67	3.40	1.73	1.64	3.36	1.74	1.64	3.37

3.1.3 Electron configuration

Atomic magnetic moment is the consequence of electron configuration at its atomic site. In the analysis of PDOS, the 3d electron configuration is tabulated for the inverse B in Table 3.3. These numbers of electrons are estimated within each atomic region. Therefore, the electron outside atomic region is excluded from the value. Compared between the results of GGA and QSGW, several features are pointed out. First, the number is decreased at cation 3d sites and O 2p sites. Second, the number of atomic majority (minority) spin state increases (decreases) at Co_{Td} 3d and Ni 3d. {Both features result} in the increase of magnetic moment on Co_{Td} 3d and Ni 3d.

The electron configuration of atom in solid crystal may not be the best way to represent using the ionic representation for cation elements. However, such a way is helpful to understand pictures of electronic state more deeply. As a speculation, the electron cofiguration at the atomic state may be presented as Co(Td) 3d $(d\uparrow)^5(d\downarrow)^2$, Ni 3d $(d\uparrow)^{3.5}(d\downarrow)^5$, and Co 3d $(d\uparrow)^{3.5}(d\downarrow)^{3.5}$.

TABLE 3.4: Total and projected DOS $N_{\downarrow}$ at E_F (states/eV/cell) in inverse B from GGA and QSGW. At the row of "O 2p", all O 2p contributions are included and at the row of "Sum" the summation of atomic values are reported.

$N_{\downarrow}(E_F)$	GGA	QSGW
Co(tet) 3d	2.45	3.50
Ni (oct) 3d	0.92	0.16
Co (oct) 3d	0.82	0.42
O 2p	0.82	0.53
Sum	5.01	4.61
Total	5.67	6.15

3.1.4 Properties at the Fermi level

The electronic states near the Fermi level consist mainly of the 3d-orbitals on Ni(oct) and Co(oct) in the majority spin state, and of the 3d orbitals on Co(tet) in the minority spin state. In Table 3.4, the total and {partial DOS} at the Fermi level (inverse type B) are reported for GGA and QSGW. The total DOS is similar to each other and the main cotribution is from Co(tet). However, there are remarkable difference on its component. The components of Ni(tet), Co(oct), and O decreases from GGA to QSGW, {whileas} the component of Co(oct) increases. These changes on the component implies a large change at electronic state of the Fermi level.

From band dispersion curves at Figure 3.1, two bands cross the Fermi level at the minority spin state. As a consequence, there are two Fermi surfaces, as depicted in Figures 3.5. As shown, the Fermi surface is not so large that they extends to a large volume in the first Brillouin zone (**k**-space).

For majority spin, the band structure shown non- metallic property. GGA shown the largest band width of 2.4 eV. QSGW method resulted in about 2.1 eV band width, while One-shot QSGW gave the smallest band width of 1.9 eV . GGA, one-shot and full QSGW methods shown separation of valence bands into two smaller bands, separated by 0.4 , 1.0 eV and 0.2eV respectively. The band width of the these sub-bands are greater in GGA methods, compared to the others. The upper sub-band (near Fermi level) of QSGW method shown no further separation, in contrast with one-shot QSGW and GGA results. The total densities of states (DOS) of full inverse NiCo2O4 spinel also calculated using the same methods, shown in figures ??, on the same set with the PDOS of Ni 3d, Co 3d and O 2p orbitals.

The total and PDOS at E_F using all methods are listed in table ??. The

smallest total DOS at E_F is produced by GGA method. However, all method agree that the PDOS at E_F is largely contributed by Co 3d at Tetrahedral position. On this account, it is proper if we decide to heavily consider Co 3d in further discussion on physical properties in which the electronic states near E_F play important roles, i.e. transport properties. The PDOS of Co 3d at E_F contributed by each tetrahedral (Co_{Td} 3d) are 2.453, 11.150 and 3.499 states/eV calculated using GGA, QSGW0, and QSGW respectively. This value is compared with 1.9845 states/eV/atom of FCC Co in non-magnetic state at ferromagnetic order. The electronic states at E_F is mainly contributed by Co_{Td} 3d states.

3.1.5 Nature of hybridization between metallic 3d orbitals and O 2p

From atomic PDOS, we can see that O 2p orbitals are strongly hybridized with metallic 3d in wide energy range of around 8 eV. To understand this hybridization, we calculated the PDOS of eg and t2g component of 3d orbitals. The results are shown in figure **??**. We specify the symbols of orbitals need to understand the details at Computational Quantum Chemistry II: The Group Theory Calculator. This description is also reinforced by weighted band dispersion curve that generated from those orbital components.

From Figure f04.d.psigmaO.invB.QSGW, we found no trace of fat-band identified at around 2eV. Figure f04.d.ppiO.invB.QSGW also shows no raising band. This indicated that we need to find that particular path.

From atomic PDOS, we can see that O 2p orbitals are strongly hybridized with metallic 3d in wide energy range of around 8 eV . To understand this hybridization, we calculated the PDOS of eg and t2g component of 3d orbitals. The results are shown in figure ??. We specify the symbols of orbitals need to understand the details at Computational Quantum Chemistry II: The Group Theory Calculator . This description is also reinforced by weighted band dispersion curve that generated from those orbital components.

Due to half-metallic nature of this structure, we see different profile of band structure between Majority and Minority spin. From Figure **??**, we see that O 2p orbital in GGA unoccupied bands, seems to hybridize with both Ni 3d and octahedral Co 3d in the width range of about 1 eV. However, from QSGW and One-shot QSGW results, we found that this hybridization got separated between O 2p-CoOct 3d hybridization at lower energy unoccupied bands and O 2p-Ni 3d at higher energy unoccupied bands. PDOS on 2p component of

O at figure **??** shows that lower part of conduction band is contributed by O-2p_{pi} that hybridized with 3d of octahedral Co. On the other hand, the higher part of conduction band is mainly formed by O-2p_{sigma} that hybridized with Ni 3d. We can suspect that the nature of these two bonds are anti-bonding. Tetrahedral Co 3d shown different band profile, as expected from different nature of 3d orbital between Tetrahedral and Octahedral configuration, based on Crystal Field Theory.

More detailed PDOS on 3d components of Ni and Co(Oct) at Figure **??**, revealed more complete view of these bonds. From figure **??**, we can identify that two components of Ni 3d orbitals are hybridized into unoccupied bands at around 2eV. The other two are hybridized into occupied states, while one component in occupied state stand alone at slightly different energy range than the other occupied twos. However, the more detailed nature of this hybridization can be understood from the fat-band shown at figure f04.d.ppi-egCoOct.invB.QSGW. This figure emphasize the nature of hybridization between O-ppi and 3d-eg of Octahedral Co. Furthermore, the isosurface of orbitals at k-point X at energy range around 1eV in figure smrho.ppiO-egCoOct.invB.QSGW, revealed the anti-bonding nature of this 3d_{eg}-p_{pi} hybridization. This anti-bonding hybridization at the same time give raise as an evidence for the covalent nature part of Co-O bonds, instead of fully ionic or metallic. On the higher energy part of conduction band, we can identify the hybridization between 3d_{eg}Ni with p_x-O, that we confirmed further as an axis for sigma bonding. Quantitatively, the contribution of 3d_{eg}Ni ratio with p-O is much larger than that in Co-O hybridization. This brings to our conclusion that the covalent character of Co-O bonding is higher than that of Ni-O. On the other hand, the addition of electron would give rise to the occupancy of anti-bonding of Co-O pi orbital, while Ni-O sigma anti-bonding orbital would filled at higher energy. This is as expected as pi bonds have lower strength than sigma bonds. We also supposed that there is asymmetric pi-backbonding happened in between covalent part of Co-O-Ni bondings.

To understand the covalent bonding nature of this structure, we need to look into valence band of the majority spin. In valence band of the majority spin, we found that the highest energy band is contributed by 3d of octahedral sites (consisted of Ni and Co). The lower energy band of this band is contributed by 3d of Co(tet). Both bands have significant contribution from p orbital of O as an indication of small covalent character that previously detected at conduction band. However, the majority of O-p orbitals filled energy range of approximately 5eV width.

At majority level, we have octahedral sites (Co and Ni) gave the highest contribution on the quasi-insulating characters. However, at minority level, the metallicity is mainly contributed by tetrahedral sites (Co_{Td}). Interestingly, the magneticity is contributed as an anti-ferro configuration between tetrahedral sites (Co_{Td}) and octahedral sites (only from Ni). These electro-magnetic contributions are summarized at table .

To determine the k-point for bond discussion, we take a bond axis orientation. In this case, we take the Octahedral position (we choose one of the fewest atoms, put Ni for binding to O2p-σ, the hope is that O2p-σ will hybridize with Ni3d-z2 or Ni3d-eg). Then we check the equivalent band structure or fatband for Ni and O. Then look for one that produces the appropriate band-split. There should be a weight for p on O. Data needed for fat-band: O 2p pi @ p1: p2, O-2p sigma @ p3, Ni 3d @ eg temporarily, we decide that smrho will be based on X coordinates, given At this point, there is a direct band gap.

From Figure f04.d.psigmaO.invB.QSGW, we found no trace of fat-band identi- fied at around 2eV. Figure f04.d.ppiO.invB.QSGW also shows no raising band. This indicated that we need to find that particular path. Due to half-metallic nature of this structure, we see different profile of band structure between Majority and Minority spin.

From Figure ??, we see that O 2p orbital in GGA unoccupied bands, seems to hybridize with both Ni 3d and octahedral Co 3d in the width range of about 1 eV. However, from QSGW and One-shot QSGW results, we found that this hybridization got separated between O 2p-CoOct 3d hybridization at lower energy unoccupied bands and O 2p-Ni 3d at higher energy unoccupied bands. PDOS on 2p component of O at figure ?? shows that lower part of conduction band is contributed by O-$2p_{\pi}$ that hybridized with 3d of octahedral Co. On the other hand, the higher part of conduction band is mainly formed by O-$2p_{\text{sigma}}$ that hybridized with Ni 3d. We can suspect that the nature of these two bonds are anti-bonding. Tetrahedral Co 3d shown different band profile, as expected from different nature of 3d orbital between Tetrahedral and Octahedral configuration, based on Crystal Field Theory. More detailed PDOS on 3d components of Ni and Co(Oct) at Figure ??, revealed more complete view of these bonds. From figure ??, we can identify that two components of Ni 3d orbitals are hybridized into unoccu- pied bands at around 2eV. The other two are hybridized into occupied states, while one component in occupied state stand alone at slightly different energy range than the other occupied twos. However, the more detailed nature of this hybridization can be understood from the fat-band shown at figure f04.d.ppi-egCoOct.invB.QSGW. This figure emphasize

the nature of hybridiz- ation between O-ppi and 3d-eg of Octahedral Co. Furthermore, the isosurface of orbitals at k-point X at energy range around 1eV in figure smrho.ppiO- egCoOct.invB.QSGW, revealed the non-bonding nature of this $3d_{eg}$-p_{π} hybridization.

Considering that both Ni and Co(Oct) occupied octahedral sites, we can expect that the nature of this d-p hybridization is dpσ bonding. consideration on nature of Co(tet) 3d hybridization consideration on Metal-Metal interaction From these data, we can consider the nature of d-p hybridization ought to be ??? bonding. check the difference with GGA and QSGW0 results.

3.1.6 Comparison with LDA+U

The LDA+U approach has been used in the calculation of electronic structures for a lot of oxide materials. The necessary U_{eff} parameter is usually extracted from the {empirical data}. The recent work by Shi *et al.*, in which such parameters were determined in a first-principles approach, is a rare case. It can be stressed that the QSGW is a non-empirical approach. Here, we point out several differences with the LDA+U results for $NiCo_2O_4$. The LDA+U provides a set of merged bands[2, 5, 23], while the QSGW provides a set of separated bands, for examples, at the unoccupied state in the majority spin state (see Figures 3.2) and at the occupied oxygen state. On Ni(oct), the energy splitting between t_{2g} and e_g seems to be different {between} the majority and minority spin states. These differences should be further verified by advanced theoretical or experimental approach.

3.1.7 Comparison with $NiCo_2S_4$

[Total and Atomic Magnetic Moments (`\muB{=latex}`) in single irreducible cell consisting of 2 formula units, magnetic properties denoted as ferro, ferri, anti and non for ferromagnetic, ferrimagnetic, antiferromagnetic and non-magnetic respectively.]

Sites	nickel cobalt oxide Atoms	GGA	QSGW	nickel cobalt sulfide Atoms	GGA	QSGW	Atoms	GGA	cobalt oxide QSGW	Ref[10]
A $_1$ (Td)	Co	1.92	2.29	Co	0.0	0.0	Co	1.74	1.96	2.631
A $_2$ (Td)	Co	1.92	2.29	Co	0.0	0.0	Co	– 1.74	–1.96	– 2.631
B $_1$ (Oct)	Ni	– 0.72	–1.14	Ni	0.0	0.0	Co	0.00	0.00	0.00
B $_2$ (Oct)	Ni	– 0.72	–1.14	Ni	0.0	0.0	Co	0.00	0.00	0.00
B $_3$ (Oct)	Co	0.07	0.06	Co	0.0	0.0	Co	0.00	0.00	0.00
B $_4$ (Oct)	Co	0.07	0.06	Co	0.0	0.0	Co	0.00	0.00	0.00
Oxy-gen	O	0.02	0.04	S	0.0	0.0	O	0.01	0.08	0.00
Total	Ferri	4	4	Non	4	4	Anti	0	0	0

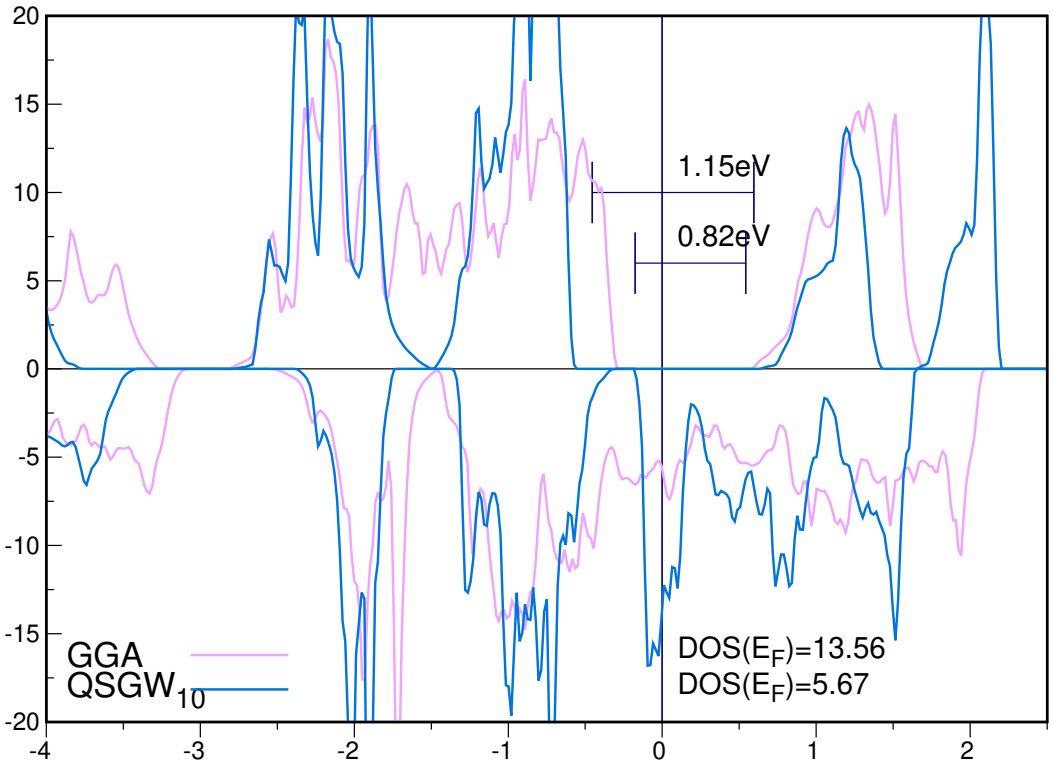

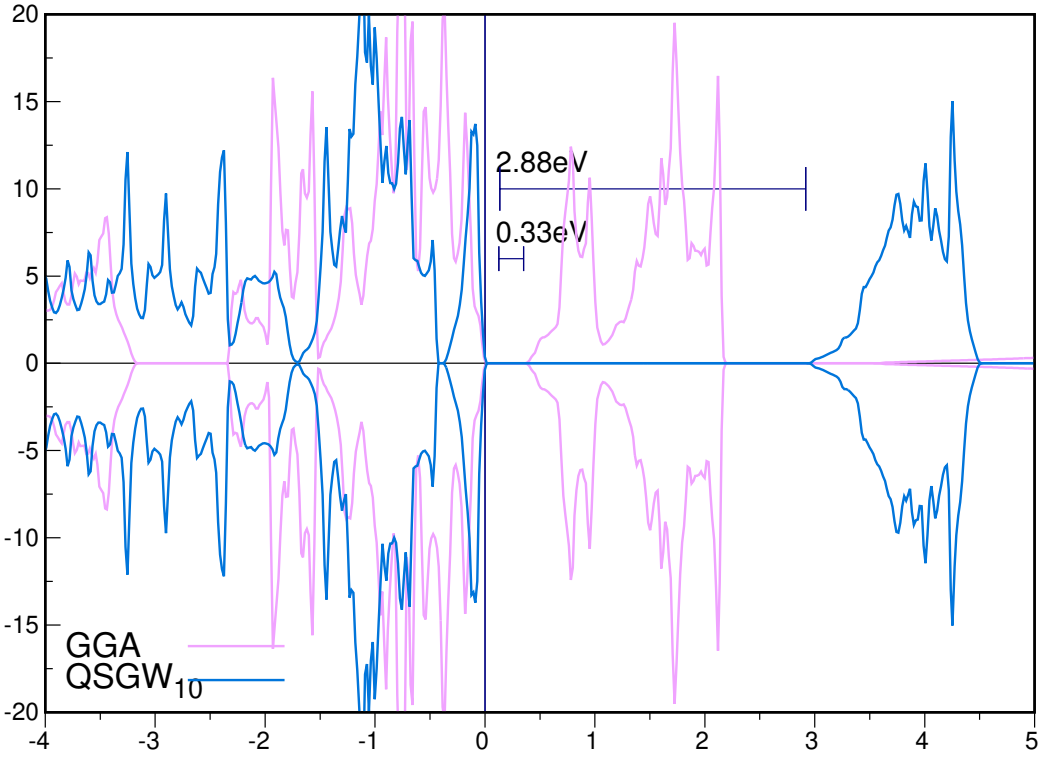

Here, we have shown at Figure **??** energy gap around E_F (eV) for Inverse B $NiCo_2O_4$ are 0.82 (GGA) and 1.15 (QSGW). This should be compared to experiment value of 2.58 eV. For Co_3O_4 in Figure **??**, we found that QSGW produced much larger energy gap of 2.88 eV, compared with 0.33 eV from GGA results. This energy gap is comparable with experiment value of 2.9 eV. QSGW systematically enlarge the pseudo-bandgap at majority spin. For Co_3O_4, we have an antiferromagnetic configuration with zero total magnetization. Here, QSGW shows its quality in predicting better band gap for semiconducting Co_3O_4.

Antiferromagnetic nature of Co_3O_4 coming from 3d orbital of Co at both tetrahedral sites. Octahedral sites of Co_3O_4 have zero contribution on magnetization. QSGW predicted that 3d orbital of Co at tetrahedral sites is fully occupied. This is in accordance to the tendency of QSGW for showing more localized electrons than GGA. On the other hand, Co(Oct) of $NiCo_2O_4$ shows similiarly small contribution to magnetization. The main contribution to magnetization in $NiCo_2O_4$ comes from both Co(Oct) and Ni(Td), with the later atoms have the highest contribution. However, conductivity of $NiCo_2O_4$ is indicated to be mainly contributed by Co at tetrahedral sites. Crystal field of metals at A and B sites also visible.

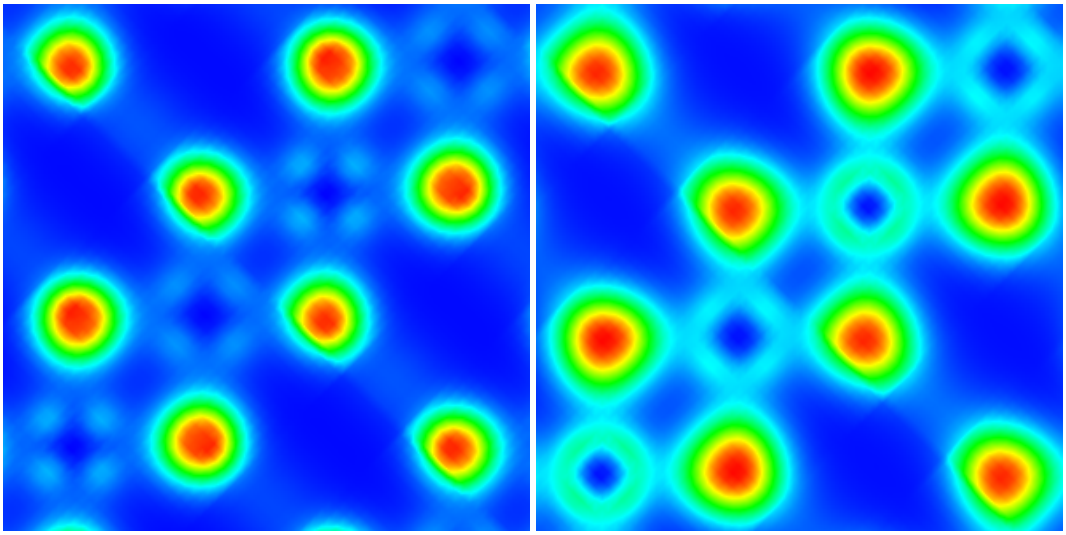

\\ 001 plane

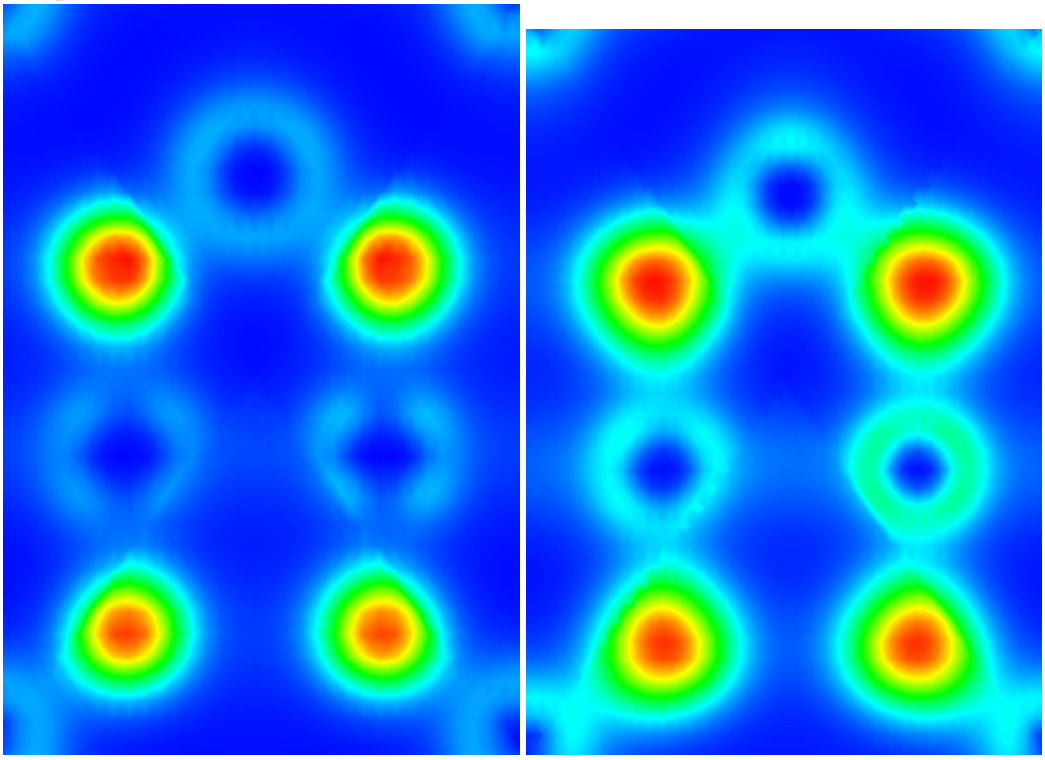

\\ 110A plane

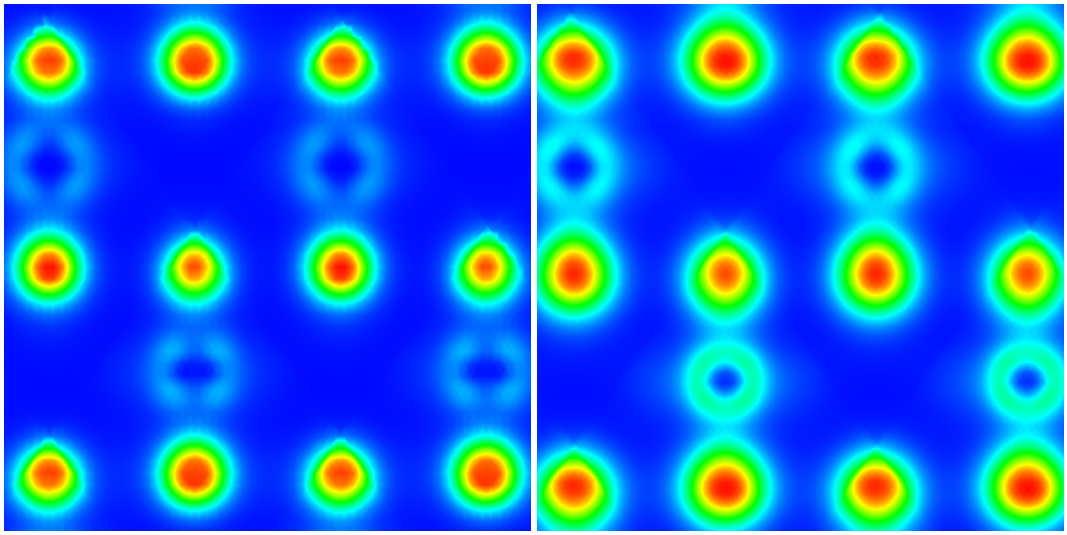

\\ 110B plane

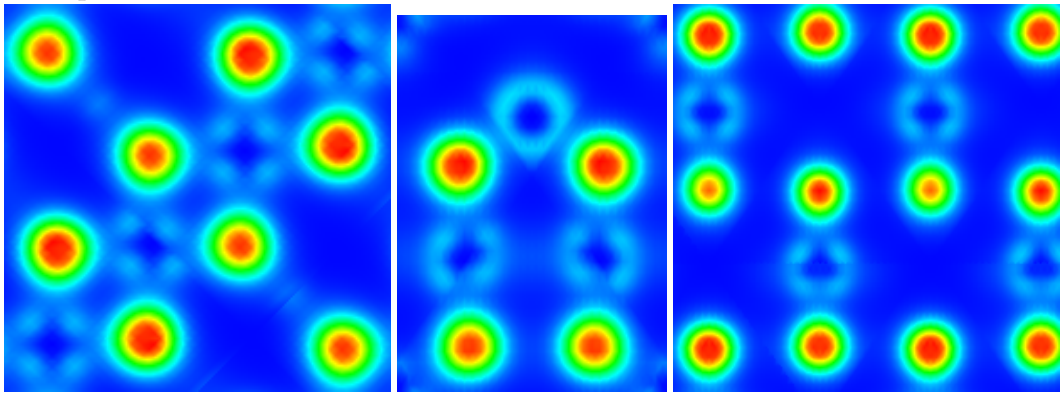

\\ 001, 110A and 110B planes of Co_3O_4

In this figure, red denotes the most negative charge, and blue means positive charge, while yellow is a transition in between. Upper part are charge density of $NiCo_2O_4$ and $NiCo_2S_4$ respectively, while at the lower part we have those from Co_3O_4. At (001) plane, we can identify covalent charges between B sites and O. This is an indication of a hybridization between B sites and O. Comparing different atoms residing B sites (Co and Ni), we can see that covalent charges is stronger or Ni-O rather than that of Co-O.

This is as expected, because the electronegativity difference between Ni-O is a little bit smaller than Co-O. Comparison between A sites and B sites can be seen at (110) plane. Here, we have Co at the top of the arc-like structure occupy A sites, while B sites are located at its both legs. From this figure, Co(Td)-O covalent bond have the lowest covalent charges.

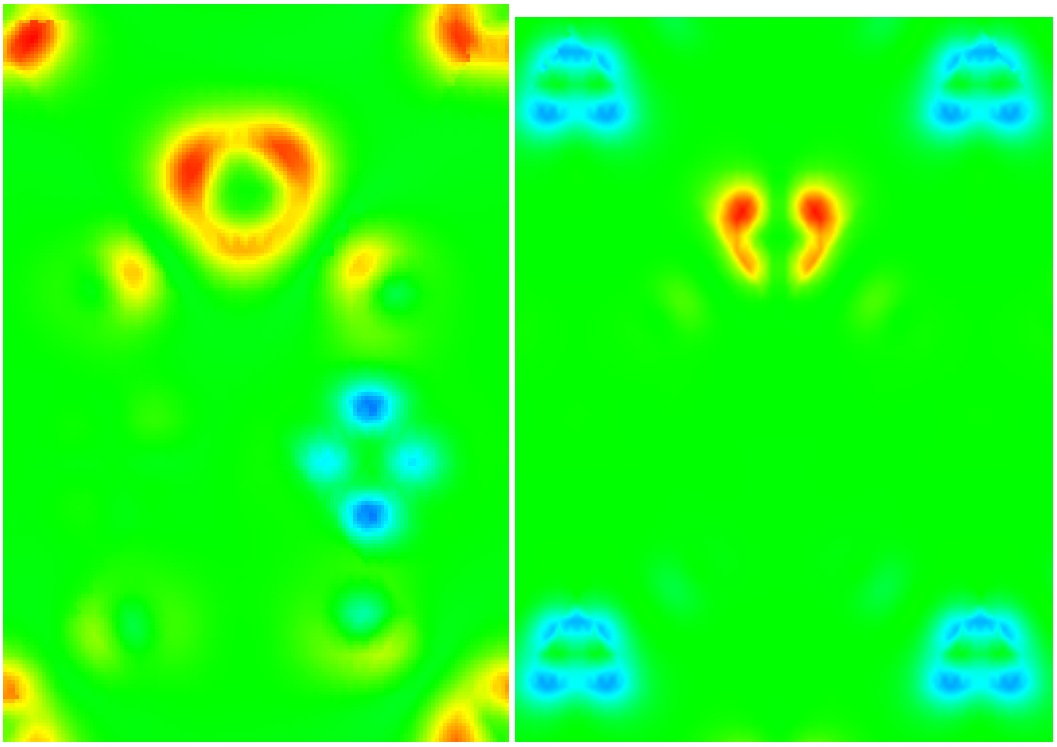

This density is generated by taking the density difference between minority and majority spin at all space. From this density, we can see that in $NiCo_2O_4$, Co(Oct) have no contribution to the magnetization, in agreement with the results of Partial Density of States. Furthermore, Ni atoms are in antiparallel with Co(Td). We also notice the strong dϵ orbital character shown by Ni. On the other hand, ferrimagnetic property of Co_3O_4 comes from antiparallel spin between two tetrahedral sites.

3.2 inline-fortran

3.3 CPVO in Haskell

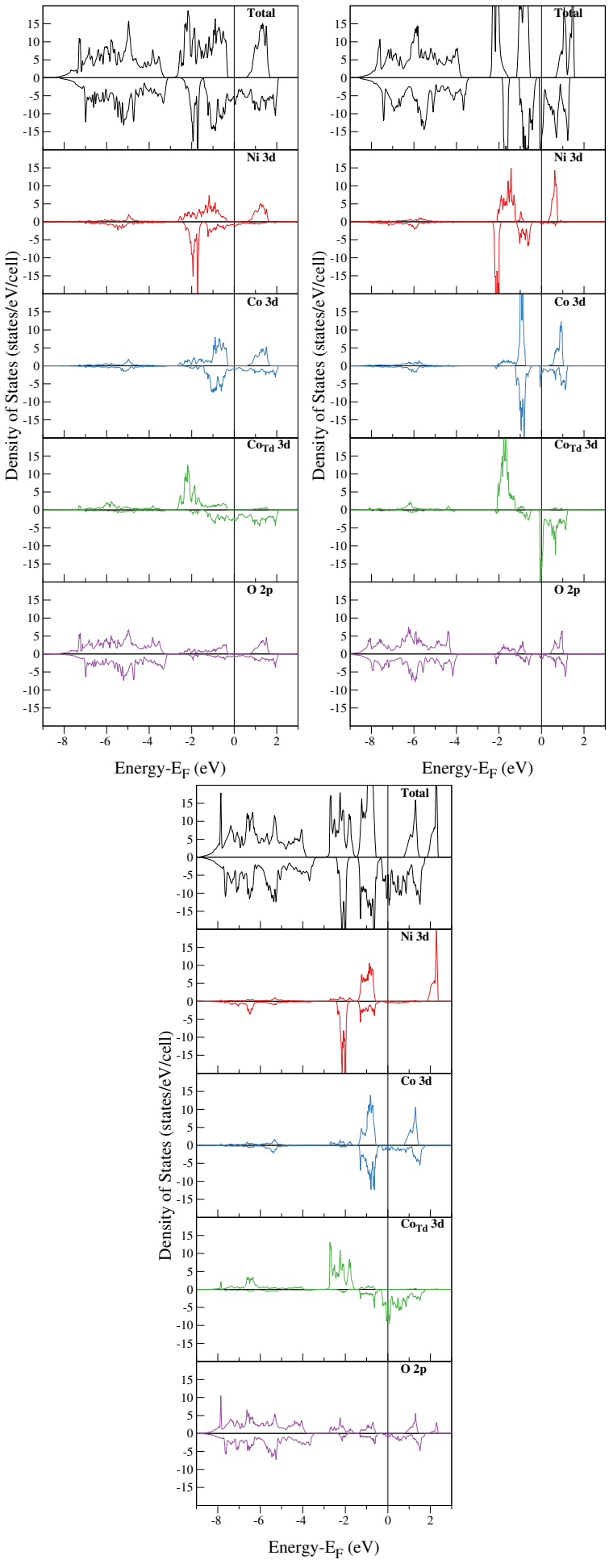

FIGURE 3.2: Total and projected densities of states (DOS) of the Ni(oct) 3d, Co(oct) 3d, Co(tet) 3d, and O 2p orbitals of inverse type B spinel $NiCo_2O_4$ for GGA, one-shot GW, and QSGW.

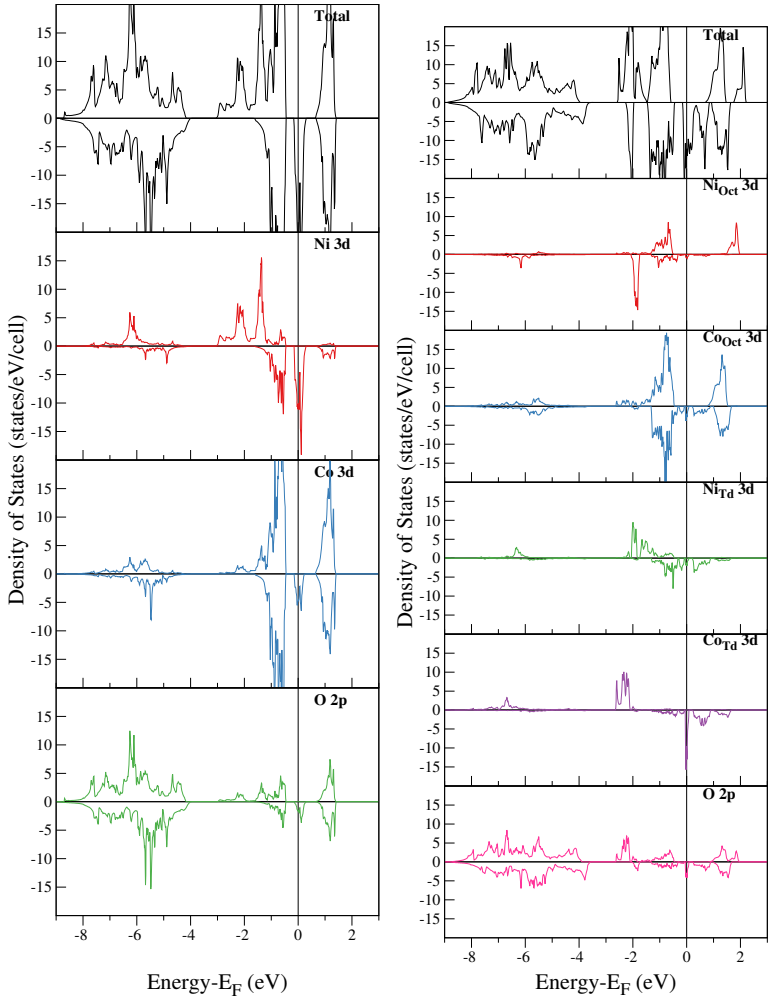

FIGURE 3.3: The total and projected densities of states of the Ni 3d, Co 3d, and O 2p orbitals of normal spinel (left) and inverse type A spinel (right) of $NiCo_2O_4$ from QSGW.

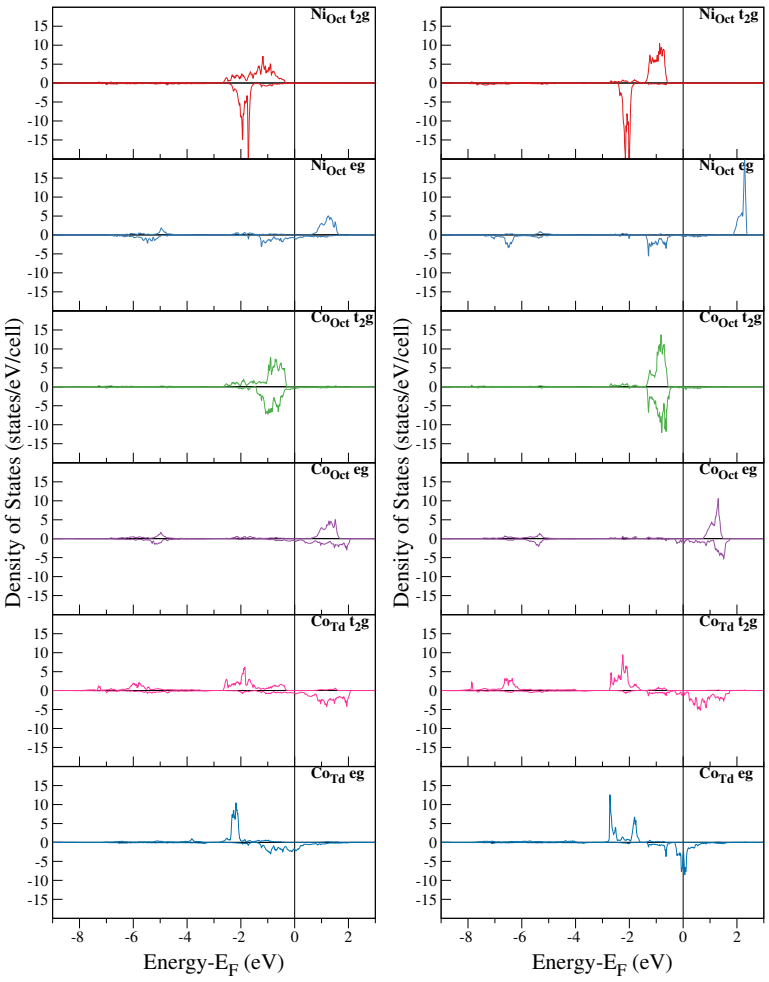

FIGURE 3.4: t_{2g} and e_g components for projected density of states on Ni 3d and Co 3d orbitals in inverse type B spinel of $NiCo_2O_4$ from GGA and QSGW.

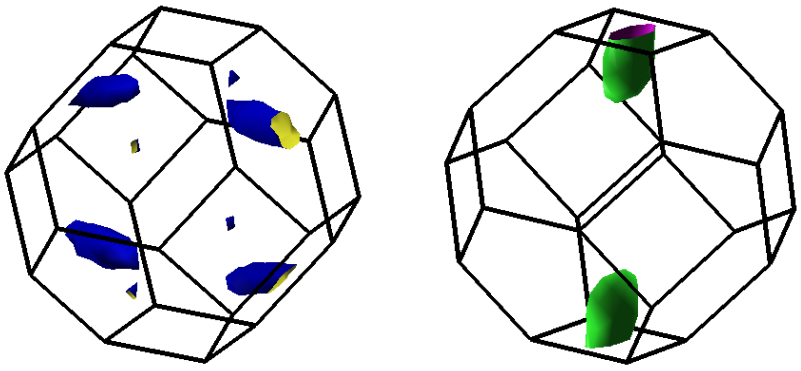

FIGURE 3.5: Fermi surfaces in inverse type B spinel of $NiCo_2O_4$ from QSGW.

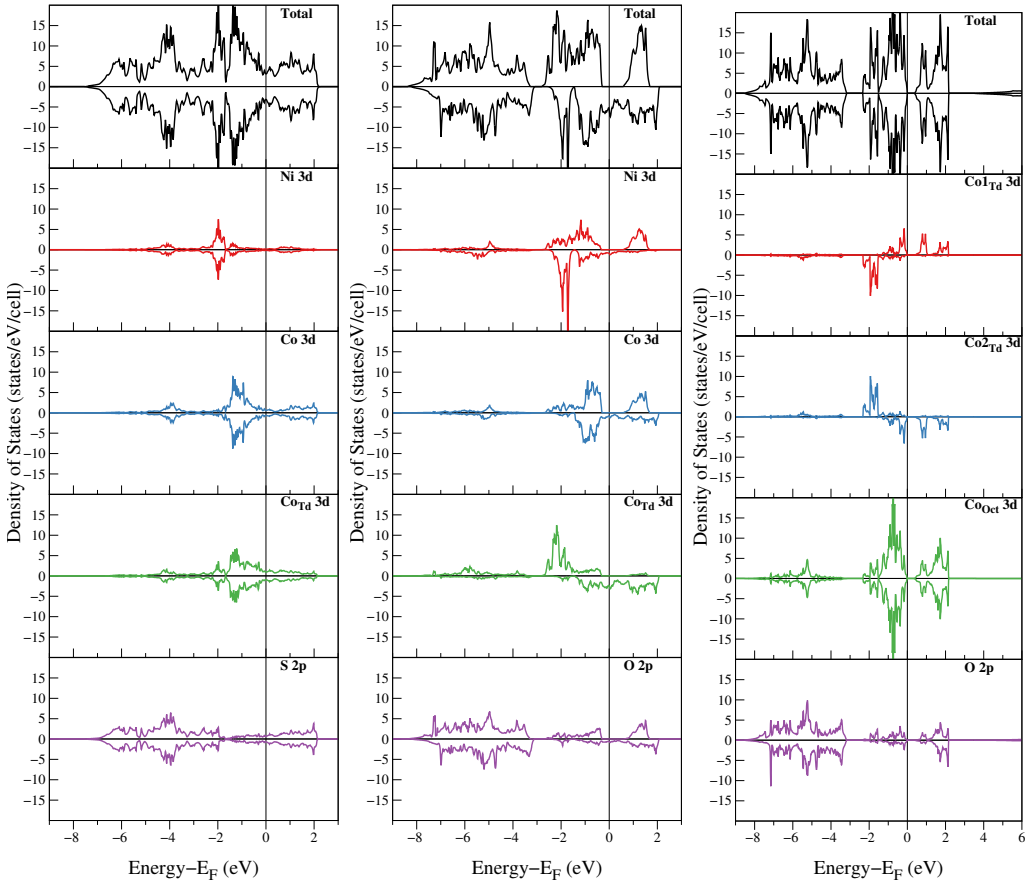

FIGURE 3.6: DFT/GGA Partial Density of States (PDOS) for inverse spinel $NiCo_2S_4$, inverse spinel $NiCo_2O_4$ and Co_3O_4, respectively from left to right.

Appendix A

Functional Paradigm in Programming Language

A.1 Language for interaction with Computer

Formal language (L) is defined by an alphabet and formation rules. Here, alphabet means a set of symbols that builds the language L. While the formation rules consisted of all specification that judge any arrangement of symbols as well-formed. From here on, the well-formed arrangement of symbols usually called words, expression, formulas, or terms. For any language L, these formation rules would specify the expressions belong to the language L. Other formation rules would specify howto build well-formed expressions from other expressions in language.

In light of this most basic definition, a programming language is a formal language that consisted of a set of instruction that conveys a human intention for a computer to do some activities. This activity is primitively seen as a flip of switch in the computer, that builds up to a much more complex activities such as showing a character on a screen or doing a complex calculation. There are different kinds of instruction set as much as different kinds of programmable machines available in the world. Today, we have x86 instruction set (and its family members, i.e.~AVX-512, SSE, and so on) that originated from Intel' s x86 microprocessor and its derivatives. On a more niche market, we also have MIPS, ARM, AVR, etc. processors that comes with their own instruction sets. A programming language can be as simple as a direct translation of machine codes to its related operation specified by its instruction sets (i.e.~Assembly language). It is important to consider what programming language that can be translated into our machine' s instruction set. A process of translating documents written in a particular programming language to those in instruction set suitable with a processor is called compilation.

From human perspective, a programming language have two components, syntax and semantics. Syntax specifies the combination of symbols that are considered as correct (well-formed), thus can be compiled. On the other hand, semantics holds our true intent on the expression. An analysis on semantics can help us to better understand what a program is doing, to optimize a program/statement, to mathematically prove that said optimization, etc. As an illustration, we can have `let var1 = if True == True then v1 else v2` and `let var1 = v1` as both well-formed, uses different syntax but have same semantics. We consider that the latter expression is more consise (it has less symbols) and more optimized (after compilation, it has less instruction set). One of the aims of programming language development is to automate the conversion of the first expression into the second. On many occasion, we found that a well optimized program is usually not so concise and subjectively not so easy to understood.

Generally, we view programming languages either as imperative (i.e.~sequence of instruction) or declarative (i.e.~specification of desired results). All programming language are implemented imperatively at hardware level (as processor' s instruction sets). The concept of imperative paradigm can also be found in recipes, checklists, workflow, etc. In imperative paradigm, each step is an instruction that flows from the beginning of a program to its end (control flow). These instructions can be an assignment, that is an operation of storing information into memory. In higher level languages, a single step of assignment can be consisted of more complex expression, such as arithmetic operations and function evaluations. Branch statement signifies a change of execution flow to other part of the program instead of to the default next step in line. This branch statement may be unconditional (popular as goto statement) or conditional (if statements). In its implementation, all type of conditional branches (case statements, if, if-else, multiple-ifs, etc.) is a variation of an evaluation of predicates (i.e.~v1 equals v2) followed by a goto. A loop statements (such as for loops, while loops, do-while loops, etc.) semantically is a more specialized branch statement. In a loop, the goto target is located in previous instruction (can be more than a single step before). In this case, the steps of evaluation (and its subsequent goto) can be evaluated more than once. Procedure calls, subprograms or subroutines are specialized form of unconditional branch statements that the goto target is a set of steps that ended with an instruction to go back to the next step of its caller position (return statement). This brings us to a concept of blocks, and allows us to express a complex program structure as a composition of several simpler procedures. These imperative basic concepts are

implemented as a core specification of Assembly language. FORTRAN (along with C, Basic, etc.) is implemented as a well constructed abstraction of this specification.

Declarative programming paradigm express the logic of a computation without its control flow. There is a strong tendency to make a clear correspondence between the declarative programming language and mathematical logic. In declarative paradigm, we abstracted out the *machine-like* instructions/steps and describe the desired results or formulas instead. A regular expression `` `s/Quantum-physics/quantum/g` `` is a declarative statement in light of it abstracted out any imperative steps needed. In this paradigm we have functional languages, logical languages, etc. One advantage of declarative paradigm that it allows us to implement mathematical model of physical systems in a more consise manner. The code would contains a set of equations that declare the behavioral relationships, instead of imperative assignments.

A.2 Turing completeness

A.2.1 Church-Turing Thesis

Example of implementation in Declarative and Imperative paradigm

A.3 Haskell

One of programming language that strongly implements declarative paradigm is Haskell. This language enforces functional programming with strict type systems. As a language much different with imperative programming languages, we need to open our perception on some fundamental concepts where Haskell is built on.

A.3.1 Lambda calculus

Lambda calculus was constructed and first developed by Alonzo Church as an attempt to formalize mathematical functions as a means of computation [24]. It developed further into computability theory, coined as a proof that the lambda calculus and the Turing machine have exactly the same computational power. In this sense, any set of functions that are effectively computable by the Turing machine, actually are computable by the lambda calculus. This equivalence, is deemed as very fundamental and important in development of programming languages, in such that it popularized as the *Church-Turing thesis*

[25]. Lambda calculus identify two aspects of a function (either mathematical or programmatical): 1. function is a mathematical object, a set of ordered pairs from domain and range. 2. function is an abstract black box that can take input and produces output.

From here, people can construct a mathematical theory on the meaning of computer programs (denotional semantics). The Functional Programming Language is an explicit product of a mission to turn lambda calculus into a practical programming language. One of the most renowned product of this effort is Haskell Programming Language. Haskell, in particular ghc (Glasgow Haskell Compiler), generates a computer software by following these steps: 1. Source desugaring. 2. Transformation to System F (a version of lambda calculus). 3. Translation of System F to machine language using graph reduction. At this point, it is important to understand some basics on lambda calculus.

Inside the construction of Lambda calculus, in its simplest classification, a language has constants, variables, applications and functions. All these components can be arranged to make a statement/expression. A constant is a definitive value, can be a number, a character, a string, or a value of more complicated data types. A function is a set of expressions that performs a desired task. Furthermore, an application is a statement to invoke a function. In lambda calculus, the rule of this arrangement can be expressed as:

```
exp
  = const
  | var
  | exp exp
  |   var → exp
```

For variables, its occurence in an expression can be defined either as bounded variables or free variables. In `x → x^2 + x + 1`, we have `x` bounded by the `x` (lambda expression of x). In `y - 1`, we have free variables of `y`, this means for a complete statement, `y` have to be defined somewhere else. Thus in this construct, bounded variables can only be occured if it has a lambda expression that binds it. Otherwise, we have free variables. In lambda calculus, we have three conversion rules to perform computation. These conversion rules allow us to substitute an expression with another. When a conversion produce a simpler expression, we call this as a reduction.

While the mathematical definition and proof of these rules are beyond the scope of this discussion, we can convey its practical use. The first rule is alpha conversion. This rule let us consistently change a function parameter' s

name. For example, we may have `(x → x+1) 3` become `(y → y+1) 3`. Here we change x into y. Next rule would be Beta conversion. This rule related with how we apply a functions. To operate an argument into a function (as a lambda expression), we take the body of the function and replace each bound occurence of the variable with the argument. For example, `( x → y + 5*x) 3` would be evaluated as `y + 5*3`. The last rule is Eta conversion. In this rule, for any function, we always have an equivalent of an application of lambda expression to an argument. For example, for any function f, we have an equivalent lambda expression of `( x → f x)`. In a more concrete example, we may have a function of `(+2)`. It has equal lambda expression of `( x → (+2) x)`. These two functions can be applied to an argument, i.e. `31`, resulting `( x → (+2) x) 31` and `(+2) 31`. Both expressions are semantically equal (have the same meaning). Eta conversion usually used to simplify an expression by removing a common trailing argument. For example, we have $f_1xy = f_2y$. We may convert this into $f_1 = \lambda x \rightarrow (\lambda y \rightarrow f_2y)$, the lambda expression of λy can be converted using beta conversion into $f_1 = (\lambda x \rightarrow f_2) = f_1x = f_2$. So we have $f_1x = f_2$ as equivalent functions. Practically, we can *factoring out* the last argument y from the expression. By employing these rules, we may come to a more concise code. At the same time, we can reduce the burden on managing the code. These rules seems very simple and may be guessed and accepted as a common knowledge nowadays. However, historically, the representation of an algebraic manipulation using such reduction, have been reported since early 800 CE. Contrasted with current approach in solving algebra, the imperative instruction presented by Al-Khawarizmi [26] would seems discursive, hard to follow, and needs a longer debugging session to deliver a good instruction. Though semantically, both instruction produce the same results. This is an apparent illustration of the power of symbolic and descriptive mathematical language over the imperative recipes.

A.4 First-class and higher-order functions

Higher-order functions are functions that use functions as its arguments or produce functions as a result. The common example of higher-order function is derivative function in calculus. Higher-order functions allow us to apply a function to its arguments one by one at a time, whereas in each step, we procure a new function that accepts the nex argument (a partial application/*currying*). From mathematical concepts of higher-order functions, we may define a first-class entities as any entity (i.e. number) that can correctly appear anywhere in

the program that other first-class entities can appear. Thus, first-class functions may appear as an argument or return value of other functions. This behavior can be achieved in imperative languages using function pointers. However, there are extra things to be done to reproduce the ability to do partial application/*currying*.

A.5 Pure Function

Pure functions/expression is defined as functions that have no side effects, either on memory or I/O. There are some special properties of a pure functions that may help us to optimize the code, i.e.: pure function can be removed if the result is never used. For a particular argument list, a pure function always produce a constant result (referential transparency). So there is a possibility to optimize it into a constant or caching optimization. The order of several pure functions can be reversed if there is no data dependency between the pure expressions. It also means that the functions can be performed in parallel without interfering with each other (thread safety).

The high advantage of a pure function is recognized also by imperative programming languages. To ease the optimization, Fortran includes PURE procedures as a new feature of Fortran95 standard. Most imperative language compilers also tries to automatically detect pure functions in its optimization process.

A.6 Recursion

In functional languages, an iteration is done by recursion. Recursive functions by definition is a function that at some points, calls itself. As a result, that function will be repeated until it reaches some final case. Traditionally, each iteration in a recursion would require computer to maintain some address in memory. This requirement grows linearly with the depth of recursion. In this regards, recursion is a technique that rarely used in popular programming. Nevertheless, in functional language, we may utilize a more specialized kind of recursion namely tail-recursion. The compiler can recognize and optimize a tail-recursion into the same code produced by a loop in imperative language.

A.7 Static Type system

Nowadays, functional programming languages use typed lambda calculus. The rejection of invalid code is happened at compilation time and risking false positive errors. By using algebraic datatypes, we may conviniently manipulate complex data structures. Strong static type checking at compile time provides us a more reliable program, before we implement further techniques such as test-driven development. GHC implemented a limited form of dependent types called generalized algebraic data types (GADT' s).

A.8 Category Theory

Basically, a category is simply a collection. We may define three components of a category:

- collection of *objects*
- collection of *morphisms*. Each morphism connects a source object to a target object. We denoted a morphism f that morphs a source object S to target object T as: $f : S \to T$.
- a statement of *composition* of these morphisms. Composition of two morphisms, namely $v : A \to B$ and $u : B \to C$, can be constructed as a new morphism denoted as $u \circ v : A \to C$

Category may be found in many things. The most obvious one is a Set can be called as a category of all sets. Its morphisms are standard functions and the composition would be standard function composition. A Group is a category of all groups wich have the morphisms defined as functions that preserve group operations (the group homomorphisms).

A.8.1 Category laws

Category needs to follow three laws. The composition of morphism needs to be associative. Category needs to be closed under the composition operation. Finally, there must be an identity morphism for every object A in a particular category C.

Morphisms compositions are applied right to left in Haskell (as commonly done in mathematics), so with $f \circ g$, first we would apply g and then followed by f.

The requirement that a category needs to be *closed* under composition, means that there should exist a morphism $h : A \to C$ in the category in such that for any two morphism $f : B \to C$ and $g : A \to B$, we would have $h = f \circ g$.

An identity mo

Bibliography

[1] B Chi, H Lin, J Li, N Wang, J Yang, *International Journal of Hydrogen Energy* **2006**, *31*, 1210–1214.

[2] P. Li, C. Xia, D. Zheng, P. Wang, C. Jin, H. Bai, *physica status solidi (RRL) – Rapid Research Letters* **2016**, *10*, 190–196.

[3] Y. Bitla, Y.-Y. Chin, J.-C. Lin, C. N. Van, R. Liu, Y. Zhu, H.-J. Liu, Q. Zhan, H.-J. Lin, C.-T. Chen, Y.-H. Chu, Q. He, *Scientific Reports* **2015**, *5*, 15201.

[4] G Blasse, *Philips Research Reports* **1963**, *18*, 383.

[5] K. Zhang, C. Zhen, W. Wei, W. Guo, G. Tang, L. Ma, D. Hou, X. Wu, *RSC Advances* **2017**, *7*, 36026–36033.

[6] O. Knop, K. I. G. Reid, Sutarno, Y. Nakagawa, *Canadian Journal of Chemistry* **1968**, *46*, 3463–3476.

[7] P. Silwal, L. Miao, I. Stern, X. Zhou, J. Hu, D. H. Kim, *Applied Physics Letters* **2012**, *100*, 032102.

[8] K. Dileep, B. Loukya, P. Silwal, A. Gupta, R. Datta, *Journal of Physics D: Applied Physics* **2014**, *47*, 405001.

[9] D. Santos-Carballal, A. Roldan, R. Grau-Crespo, N. H. de Leeuw, *Physical Review B* **2015**, *91*, Publisher: American Physical Society, 195106.

[10] S. V. Faleev, M. van Schilfgaarde, T. Kotani, *Physical Review Letters* **2004**, *93*, Publisher: American Physical Society, 126406.

[11] M. van Schilfgaarde, T. Kotani, S. Faleev, *Physical Review Letters* **2006**, *96*, Publisher: American Physical Society, 226402.

[12] T. Kotani, M. van Schilfgaarde, S. V. Faleev, *Physical Review B* **2007**, *76*, 10.1103/PhysRevB.76.165106.

[13] W. Kohn, L. J. Sham, *Physical Review* **1965**, *140*, A1133–A1138.

[14] J. Otsuka, T. Kato, H. Sakakibara, T. Kotani, *Japanese Journal of Applied Physics* **2017**, *56*, Publisher: IOP Publishing, 021201.

[15] A. Sawamura, J. Otsuka, T. Kato, T. Kotani, *Journal of Applied Physics* **2017**, *121*, Publisher: American Institute of Physics, 235704.

[16] H. Sakakibara, T. Kotani, M. Obata, T. Oda, *Physical Review B* **2020**, *101*, Publisher: American Physical Society, 205120.

[17] T. Oda, A. Hosokawa, *Physical Review B* **2005**, *72*, Publisher: American Physical Society, 224428.

[18] M. G. Brik, A. Suchocki, A. Kamińska, *Inorganic Chemistry* **2014**, *53*, 5088–5099.

[19] P. Hohenberg, W. Kohn, *Physical Review* **1964**, *136*, B864–B871.

[20] H. Yukawa, *Proceedings of the Physico-Mathematical Society of Japan. 3rd Series* **1935**, *17*, 48–57.

[21] L. Hedin, *Physical Review* **1965**, *139*, A796–A823.

[22] J. F. Marco, J. R. Gancedo, M. Gracia, J. L. Gautier, E. I. Ríos, H. M. Palmer, C. Greaves, F. J. Berry, *Journal of Materials Chemistry* **2001**, *11*, 3087–3093.

[23] X. Shi, S. L. Bernasek, A. Selloni, *The Journal of Physical Chemistry C* **2016**, *120*, 14892–14898.

[24] A. Church, *American Journal of Mathematics* **1936**, *58*, 345.

[25] S. C. Kleene, *Mathematical Logic*, **1967**.

[26] M. Ibn Musa, al-Kitāb al-Mukhtaṣar fī ḥisāb al-Jabr waʾ l-Muqābala, trans. by F. Rosen, **820 (1831 tl.)**